ARISTOTLE UNIVERSITY OF THESSALONIKI

FACULTY OF SCIENCES

SCHOOL OF CHEMISTRY

Erasmus Mundus Master in
ARCHMAT
ARCHaeological MATerials Science
MASTER THESIS

Novel Superhydrophobic Polysiloxane-based Materials for the Conservation of Marble

Zebunnisa Chughtai

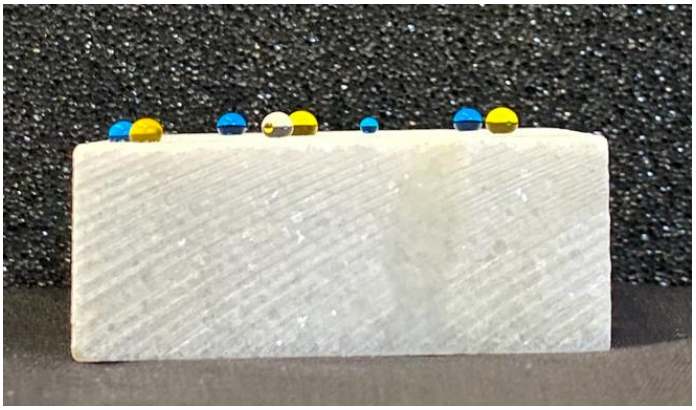

Supervisor/s: Dr. Ioannis Karapanagiotis
Dr. Panagiotis Spathis
Dr. Thodoris Karapantsios

Thessaloniki 2022

Aristotle University of Thessaloniki
School of Chemistry

ARCHMAT
Erasmus Mundus Master in ARCHaeological MATerials Science

Master's Thesis

Novel Superhydrophobic Polysiloxane-based Materials for the Conservation of Marble

Zebunnisa Chughtai (m47326, 2026068)

Dr Ioannis Karapanagiotis – Department of Management and Conservation of Ecclesiastical Cultural Heritage Objects, University Ecclesiastical Academy of Thessaloniki
Dr Panagiotis Spathis – Department of Chemistry, Aristotle University of Thessaloniki
Dr Thodoris Karapantsios – Department of Chemistry, Aristotle University of Thessaloniki

Thessaloniki 2022

This thesis has been defended on the 22nd of December 2022, in front of a jury comprising:

Professor Donatella Magri	President of the Jury, *Sapienza University of Rome, Italy*
Professor Yiannis Karapanagiotis	Supervisor, *Aristotle University of Thessaloniki, Greece*
Professor Cristina Lemorini	Member, *Sapienza University of Rome, Italy*
Professor Nicola Schiavon	Opponent, *University of Evora, Portugal*
Professor Emanuela Borgia	Member, *Sapienza University of Rome, Italy*
Professor Panagiotis Spathis	Member, *Aristotle University of Thessaloniki, Greece*
Professor Eleni Pavlidou	Member, *Aristotle University of Thessaloniki, Greece*

Abstract

Biomimetic materials with extreme wetting properties (MEWP) offer great potential as protective coatings against water-induced damage and oil-based soiling of stone-built heritage. This thesis assessed the performance of two novel coatings, one superhydrophobic, D/S/F (WCA =160.0°), and the other superamphiphobic, 6P/1F/2S (WCA=160.3°, OCA=152.2°). This involved characterizing their wettability, breathability, mechanical durability, resilience to environmental degradation agents (extreme temperature, acid/ rain, particulate matter) and response to accelerated UV-aging. Test protocols were adopted from standards, adapted from previous research, and optimized through trial runs. Particularly, the sandpaper abrasion test was applied to coatings being developed for heritage application for the first time. The D/S/F coating showed a 25% improved protection from water uptake compared to the commercial product with minimal effect on breathability (%RVP = 16%). It also demonstrated great mechanical durability across many cycles of sandpaper abrasion, tape peeling, acid rain simulation and sand-grit erosion. The 6P/1F/2S coating, however, did not offer improved protection from water penetration, with a higher associated impact on the breathability of stone (%RVP = 54%) but showed promising tolerance to freeze-thaw cycles and acid/rain simulation. Both the coatings maintained enhanced hydrophobicity over 2 months of artificial UV-aging. In summary, this research delineates the performance of two novel coatings displaying extreme wetting behaviour, while also contributing towards the development of test protocols that enable application-oriented assessment of coatings designed for the protection of stone heritage.

Table of Contents

LIST OF FIGURES

LIST OF TABLES

LIST OF ABBREVIATIONS

MEWP – Materials with extreme wetting properties

SCA – Static contact angle

WCA – Water contact angle

OCA – Oil contact angle

SA – Sliding angle

CAH – Contact angle hysteresis

NPs – nanoparticles

PMMA - Poly (methyl methacrylate)

PFPE – Perfluoropolyether

SEM - Scanning electron microscopy

O-I – Organic-Inorganic

TEOS - Tetraethoxysilane

PDMS-OH - hydroxyl-terminated polydimethylsiloxane

n-HA - nano-hydroxyapatite

PFOA - Perfluorooctanoic acid

PFOS - Perfluorooctane sulfonate

CTAB - cetyl trimethyl ammonium bromide

FPS - Fluorinated polysiloxanes

VOC – Volatile organic compound

PVC - Poly (vinyl chloride)

AC - water capillary absorption coefficient

R.H. – Relative humidity

%RC – Percentage reduction in water uptake by capillary action

%RVP – Percentage reduction in vapour permeability

ACKNOWLEDGEMENTS

I offer sincere thanks to the coordinators of the ARCHMAT consortium, Professor Nicola Schiavon, Professor Donatella Magri and Professor Panagiotis Spathis who gave me the opportunity to go on this adventure. I am very grateful to my supervisors Dr. Ioannis Karapanagiotis, Dr. Thodoris Karapantsios and Dr. Panagiotis Spathis for their guidance and offer my sincere gratitude to Dr. Panagiotis Manoudis for lending his expertise to this body of research. I am specially indebted to Dr. Vasilios Tsiridis and everyone in his laboratory who made me feel at home. Without his consistent support and presence throughout my research endeavours this work would have been impossible. I would also like to express my deep *shukar* for the undying support from Loizos Theodorou, David Alexandros Sisti and my colleagues back in Portugal, to whom I owe the magic of the past two years. I also thank my mother, Aliya Zia Chughtai, and my sisters, Mah Afroze Chughtai, Jahan Ara Chughtai, and Arjumand Bano Chughtai, for celebrating my success and supporting me always. Thank you to Arif Rahman Chughtai, as well, for gifting me with the education that brought me this far!

1 Introduction

1.1 The wetting phenomenon and cultural heritage

Historical monuments as architectural heritage have very high economic and cultural value to the country they are situated in. As survivals from our ancestors they represent a country's national identity while maintaining and enriching its extant cultural practices. Some monuments represent not just the history of a demarcated piece of land but also the shared global history of humankind. These monuments are key pieces to a puzzle that help us understand the history of humanity and need to be preserved for future generations to access. Such high priority natural and cultural sites are inscribed on the World Heritage List by UNESCO, the United Nations Educational, Scientific and Cultural Organization [1]. Consequently, the conservation of heritage monuments requires serious and unremitting effort by professionals in both the humanities and the natural sciences [2].

A large volume of the world's tangible cultural heritage lives on in the form of monuments that are predominately made from porous inorganic materials including natural stone, as well as artificial materials such as mortar, plaster, and brick etc. Unlike heritage objects protected by the controlled environment of a museum, outdoor heritage is exposed to the elements resulting in an accelerated rate of deterioration. Heritage monuments become vulnerable to many different agents of degradation as they age, particularly the pervasive and multi-faceted damage caused by the action of water.

Natural stone becomes physically and chemically vulnerable to the action of water through various mechanisms. Water causes stone deterioration through freezing and thawing cycles inside the pores of the stone, wetting and drying cycles due to rainwater and condensation, erosion by running

water in fountain settings and by intra-porous crystallization of the salts transferred by water from the environment [3]. Water also interacts with the mineral constituents of the stone causing the hydrolysis of silicate rocks and the dissolution of carbonate rocks, simultaneously releasing substances that adversely impact the stone [4]. This fluid is also an important medium for the transport of pollutants and biological agents resulting in the growth of microorganisms and the formation of a biofilm or crust on the surface of stone monuments. As a result, stone monuments suffer loss of material through weathering, as well as, chromatic and textural alterations thereby impacting the aesthetic appearance of the monument and obscuring its associated philosophical meanings.

Consequently, it is important to develop materials and strategies to protect built heritage from water in order to preempt the weathering and decay of stone and stone-based monuments. This body of work contributes to the development of conservation materials with extreme wetting properties that are capable of minimizing and inhibiting the deleterious action of water on outdoor heritage.

To develop sustainable conservation materials, the field of *biomimetics* draws inspiration from the sophisticated mechanisms and materials that occur in the natural world. A close look at nature reveals a plethora of naturally occurring materials that possess desirable wetting behaviours such as *superhydrophobicity*, the property of a surface that is energetically and structurally predisposed to make minimal-possible contact with water droplets.

There are myriad examples of naturally occurring superhydrophobicity. One typically quoted example is the “lotus effect” that is observed in the leaves of the plant species *Nelumbo nucifera* alongside many other terrestrial plants [5], [6], [7]. This effect produces a large static contact angle

between the surface and the water droplets, resulting in a characteristic rolling off behaviour. This behaviour is the result of a combination of energetic and structural features of the surface, particularly the microscale (cellular structures) and nanoscale (presence of wax crystals) roughness of the superhydrophobic surface [7], [8], [9]. An often-associated desirable behaviour is water-repellency i.e., the ability of surfaces to *self-clean* as the water droplets incident upon them roll off carrying with them any dust and impurities present on the surface. This self-cleaning ability is also exhibited by the wings of some insects [10], [11].

We delve into these phenomena further in chapter 2 but first it is important to categorize the different stone-water interactions and define the fundamentals of wettability as a physical phenomenon. This is tackled in the following section.

1.2 Fundamentals of wettability

The wetting properties of a solid surface reflect its ability to maintain contact with a liquid. This behaviour results, in part, from intermolecular interactions when the liquid and solid surfaces encounter each other. Consequently, the wettability of a material is determined by a force balance between the adhesive and cohesive forces that come into play. Wetting properties are governed by three major factors: surface energy, surface roughness, and surface inhomogeneity [12].

Wettability can be thought of as an unfolding of a liquid phase on the surface of a solid phase, thereby converting a solid-vapour interface into a solid-liquid interface. Consider a drop of liquid on a solid substrate, the thermodynamic equilibrium of the three phases i.e., solid, liquid, and vapour, determines the equilibrium shape of the liquid drop and the associated static contact angle, SCA [13]. The static contact angle, SCA, also called the equilibrium contact angle, θ, is defined as the angle the liquid makes at the three-phase boundary point with the underlying horizontal

surface [14] and can be visualized in figure 1(a). The static contact angle, SCA, is one of the core parameters used to categorize the wettability of a surface.

Figure 1: Schematics of (a) static contact angle (b) sliding angle

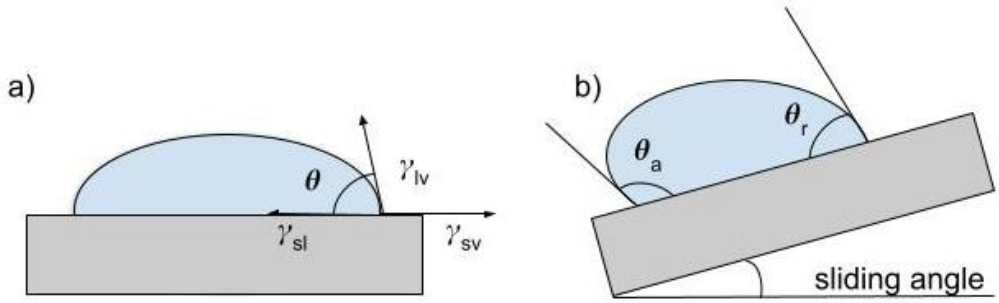

Sliding angle, SA, and contact angle hysteresis, CAH, are additional parameters that expound upon the definition of wettability. In a dynamic process, the contact angle formed in front of a forward contact line is called the advancing CA, θ_a, while that formed behind a backward contact line is the receding CA, θ_r, as shown in figure 1(b). In general, the advancing and receding angles are not the same, which gives rise to contact angle hysteresis, CAH. Hysteresis exists due to surface heterogeneity and defects and is defined as the difference between the advancing, θ_a and receding, θ_r contact angles. The sliding angle, SA, is defined as the critical angle just after which the liquid drop begins to slide on a tilted surface [13].

The SA is an important parameter quantifying the water repellence of a surface, a property related to but different from the hydrophobicity of the surface. It is possible for surfaces with very high SCAs to also possess high SAs resulting in the spherical droplet being pinned to the surface by adhesive forces instead of showing the rolling off behaviour termed “the lotus effect.” This pinned hydrophobic wetting is called the “rose petal effect” after the natural surface showing this

behaviour. Such a surface is highly superhydrophobic but retains water which can have interesting applications involving droplet retention including directional droplet transport, anti-icing, and water harvesting to name just a few [15].

Typically surfaces with SCA < 90° are classified as hydrophilic, whereas surfaces with SCA > 90° are classified as hydrophobic [16]. Recent research suggests that a lower SCA threshold of ~65° is a better criterion to distinguish hydrophilic surfaces from hydrophobic ones [17], [18]. The typical cut offs are utilized here.

Hydrophobicity can be further broken down into three regimes: weak hydrophobicity, enhanced hydrophobicity, and superhydrophobicity corresponding to 90°< SCA< 120°, 120° < SCA < 150° and SCA > 150°, respectively as shown in figure 2.

Figure 2: Classification of different regimes of hydrophobicity

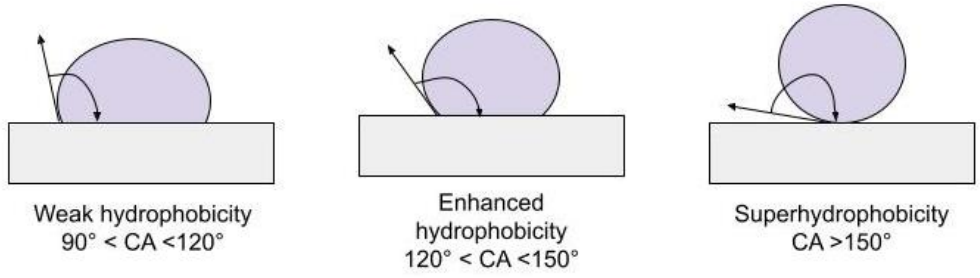

A surface is defined to be superhydrophilic if water has a SCA smaller than 5° [19].

1.3 Theoretical frameworks for wettability

This section outlines the models that attempt to explain wettability along with the limitations of their explanatory power. These are Young's model, Wenzel's model and the Cassie–Baxter model dealt with in chronological order.

1.3.1 Young's Model

The first model that attempted to systematically explain the interaction between a solid surface and a water droplet was proposed by Thomas Young in 1805 [16]. This model describes a droplet of water resting on an infinitely horizontal, passive (i.e. uninfluenced by gravity) and atomically smooth surface. The exact shape of the water droplet is specified by a force balance equation called the Young equation [20].

At the contact point of the three phases viz solid, liquid and vapour, the droplet experiences three forces: one from the solid-vapour (SV) interface, one from the solid-liquid (SL) interface, and one from the liquid-vapour (LV) interface as indicated in figure 1(a). After equilibrating, the droplet experiences a net force described by the following equation,

$$F_{sv} - F_{sl} = F_{lv} \cos\theta_{\gamma} \qquad (1)$$

Since interfacial surface tensions are the forces at play, the equation takes on its popular form as,

$$\gamma_{sv} - \gamma_{sl} = \gamma_{lv} \cos\theta_{\gamma} \qquad (2)$$

Here, θ_{γ} refers to Young's contact angle. According to this model, the fate of the water droplet is decided solely by the relative strengths of the interfacial surface tensions. To illustrate, if $\gamma_{sv} - \gamma_{sl} = \gamma_{lv}$, then $\theta_{\gamma} = 0°$ indicating superhydrophilicity. If $\gamma_{sv} - \gamma_{sl} > 0$, then $0° < \theta_{\gamma} < 90°$, indicating a case of hydrophilicity. However, if $\gamma_{sv} - \gamma_{sl} < 0$, then $90° < \theta_{\gamma} < 180°$, indicating hydrophobic behaviour. Likewise, $\gamma_{sv} - \gamma_{sl} = -\gamma_{lv}$, is the force balance that results in the highly desirable scenario in which maximum superhydrophobicity could be achieved in theory [21].

Young's model is pioneering but limited in explanatory power. This is because it factors only the chemical compositions of the liquid and the contact surface; the morphology of the latter is not taken into account to analyze subsequent wetting behaviour. Therefore, a more comprehensive

model was needed to explain the existence of superhydrophobic surfaces which are accompanied by high surface roughness [16].

1.3.2 Wenzel Model

Young's model was limited in that it failed to account for the vital role of *surface roughness* in wetting behaviours. R. N. Wenzel, in 1936, was the first to quantitatively consider the contribution of surface roughness in relation to special properties of wettability [22].

Wenzel recognized that there is a distinction between the total or "actual" surface of an interface and the superficial or "geometric" surface; the latter being the surface as measured in the plane of the interface. Wenzel writes that perfect smoothness is an acceptable assumption for liquid-liquid and liquid-gas interfaces without rigid shape. However, the solid-liquid interface presents a situation where the actual surface of contact is greater than the geometric surface due to surface roughness/imperfections. Wenzel defined a roughness factor, r, as the ratio of the actual versus the geometric surface. This dimensionless factor, r, is a number larger than unity and equals unity only for ideal flat surfaces without bumps/imperfections. Wenzel related the apparent contact angle of a water drop on a rough surface, θ^*, to the Young contact angle, θ_γ, through the roughness factor, r, as follows,

$$\cos\theta^* = r \times \cos\theta_\gamma \quad (3)$$

It is generally accepted that the liquid droplet rests on a solid surface in one of two modalities: the non-composite (liquid intrusion) mode visualized in figure 3(a) or the composite (air entrapment) mode illustrated in figure 3(b) [21]. Wenzel's model concerns itself with the former of the two modalities.

Figure 3: (a) Wenzel non-composite wetting (b) Cassie-Baxter composite wetting

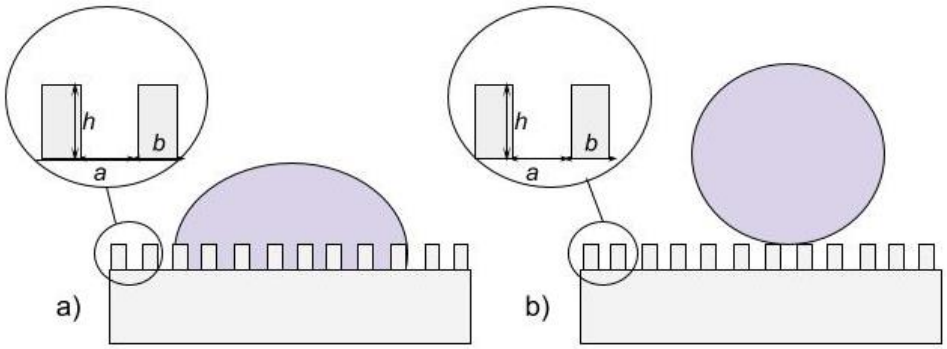

In the non-composite wetting state, the liquid fills up the grooves in the surface increasing manifold the surface area of the solid in direct contact with the liquid (edges a, b and h) compared to the composite wetting state (edge b alone). This results in the characteristic Wenzel "sticky state" as water droplets get entrapped by the surface, displaying, usually adhesive behaviour through pinning. The introduction of the roughness parameter, r, was a huge improvement over Young's model, however, the dynamic behaviour of surfaces displaying water repellency and rolling off behaviour could not be explained by this model nor by its successor [22]. Nonetheless, the Cassie-Baxter model provided further insight into static wetting behaviour and helped in modelling many different superhydrophobic materials fabricated over the last few decades.

1.3.3 Cassie-Baxter Model

In 1944, Cassie and Baxter put together a powerful model to explain the wettability of porous surfaces. The term "porous surface" illustrates that water droplets are unable to penetrate the hollows or cavities of the corrugated surface unlike in Wenzel's model. Instead, the Cassie Baxter model describes a water droplet that sits atop air pockets formed between the liquid and the solid

surface. This kind of interaction demonstrates very low hysteresis and excellent rolling-off behaviour [23].

In the composite wetting state that can be visualized in figure 3(b), the droplet rests on air entrapped inside the surface asperities dramatically decreasing the surface area of the solid in direct contact with the liquid. Decreased contact area often results in poor adhesion and the rolling-off behaviour associated with self-cleaning. The fraction of the surface that comes in contact with the top asperities is usually denoted as *f*s. This dimensionless open porosity factor, *f*s, is a number smaller than unity and equals unity only for ideal flat surfaces. According to Cassie and Baxter, the apparent contact angle of a water drop on a porous surface (θ^*) is related to Young's ideal contact angle, θ_γ through this factor (*f*s) as follows,

$$\cos\theta^* = -1 + f(\cos\theta_\gamma + 1) \qquad (4)$$

From a thermodynamic point of view, only the Wenzel state is stable, while the Cassie-Baxter scenario describes a metastable state. Hence, a transition from the Cassie-Baxter state to the stable Wenzel state is often observed.

Both Wenzel and Cassie-Baxter equations can explain the existence of contact angles higher than 150^o i.e. the defined threshold for superhydrophobicity. However, they differ in their applicability. The Wenzel model suggests that an increase in roughness increases the inherent hydrophobicity or hydrophilicity of a surface. Therefore, increased roughness results in superhydrophobicity only in the case of intrinsically hydrophobic materials. Considering that r > 1 for any surface that is not perfectly smooth, the relation in equation (3) suggests that $\theta^* < \theta_\gamma$ for inherent hydrophilic ($\theta_\gamma < 90°$) materials, while $\theta^* > \theta_\gamma$ for inherent hydrophobic ($\theta_\gamma > 90°$) materials.

In contrast, in the Cassie-Baxter model, θ^* increases with roughness (or surface porosity) irrespective of the inherent hydrophilic or hydrophobic character of the material and can therefore become $\theta^* > 150°$ even for hydrophilic materials. Considering that $f_s < 1$, equation (4) suggests that $\theta^* > \theta_\gamma$ for both inherently hydrophilic ($\theta_\gamma < 90°$) or hydrophobic ($\theta_\gamma > 90°$) materials.

The Cassie-Baxter model offers great explanatory power as intrinsically hydrophilic polymers such as PMMA have been used to fabricate superhydrophobic surfaces through surface roughening [24]. However, this model also does not shed light on dynamic wetting. For example, the rose petal corresponds to $\theta^* = 152°$ making it superhydrophobic, but "a drop cannot roll off even when the surface is turned upside down." This phenomenon is referred to as the *rose petal effect* [25]. Similarly, the high water-repellency and rolling-off behaviours of superhydrophobic surfaces such as the lotus leaf also remain uncharacterized by both models. In this way, these theoretical frameworks cannot predict whether a droplet will stick or slide in response to surface tilting which presents an altogether more complex and dynamic scenario. Nonetheless, both models are pivotal to our understanding of static wetting behaviours. However, to holistically characterize the wettability of a surface we must introduce other parameters into our discussion and expand the definition of wettability.

1.3.4 Contact Angle Hysteresis

As previously discussed, the static contact angle ($\theta*$), which describes the contact of a drop on a horizontal surface, does not adequately describe the wettability of a surface alone. A droplet on a surface with a high contact angle may remain pinned until the surface is tilted to a significant angle [26]. In 2000, Öner and McCarthy emphasized that if the goal was to obtain a water-repellent surface, the static contact angle was irrelevant beyond its role of pushing the water droplet into a

rigid spherical geometry of minimal contact. The hysteresis was more important in determining hydrophobicity than the maximum achievable contact angle. Hysteresis is a property that quantifies how readily a droplet rolls off upon tilting the surface. The smaller the force required to achieve this rolling off, the more water-repellent the surface [27].

The critical line force per unit length (F) that is needed to start a droplet moving over a solid surface is given by equation (5) as follows,

$$F = \gamma_{lv}(\cos\theta_r - \cos\theta_a) \qquad (5)$$

where F is the critical line force per unit length, γ_{lv} is the surface tension between the liquid and vapour, and θ_r and θ_a are the receding and advancing contact angles, respectively [28], [29].

Figure 4: Advancing and receding contact angles

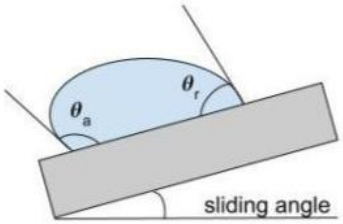

According to equation (5), as $\theta_a - \theta_r$ decreases, the critical force F needed to make the drop move decreases. Consequently, surfaces with enhanced water repellency must correspond to small $\theta_a - \theta_r$ values. This gives rise to an important parameter for the classification of wettability called *contact angle hysteresis*, defined as the difference between the advancing (θ_a) and receding (θ_r) contact angle as chosen in figure 4 [30], [31].

2 Literature review

2.1 Biomimetics

The term biomimetics was coined by American biophysicist Otto Schmitt during the 1950's and refers to the process of reverse engineering natural phenomena to mimic them in modern technology [32]. It operates off the principle that advanced materials science or structural engineering has a lot to learn from the biological models, processes and systems perfected by nature over millions of years of evolution [33].

This work more specifically concerns itself with the biomimicry of biological surfaces displaying special wettability such as superhydrophobicity, water-repellency and self-cleaning. The goal is to develop materials for the protection of natural stone used in historic monuments. To achieve this goal a well-established methodology, suited to application in the field of heritage, has been employed to develop novel coatings by enhancing the properties of commercially available polymer systems.

Interdisciplinary research in biomimetics has played a big role in the fabrication of materials with extreme wetting properties, MEWP, referring to superhydrophobic (SCA > 150° for water), superhydrophilic (SCA < 5° or water), superoleophobic (SCA > 150° for oil), superoleophilic (SCA < 5° for oil) and superomniphobic (SCA> 150° for both water and oil) materials. These MEWP are of interest due to their countless potential applications, for instance in automobiles, ships and aircrafts, microelectronics, textiles, biomedical devices and implants, devices in renewable energy systems, construction sites and buildings, and in other applications relevant to self-cleaning, friction reduction, oil–water separation, water harvesting and desalination, drug delivery, anti-icing, anti-corrosion, and anti-bacterial methods. These materials have the potential

to lead a new generation of products and devices with unique fine-tuned functionalities. In relation to this body of work, these materials have also found application in the conservation of cultural heritage by providing protection from water damage [19].

Many such materials have been fabricated over the years by heavily drawing inspiration from natural surfaces. Some examples of such natural surfaces include the lotus leaf, the peanut leaf, rose petal, the poplar leaf, butterfly wings, shark skin, the compound eyes of mosquitoes, gecko feet, spider silk, cacti and in the anisotropic dewetting of the rice leaf, among many others [34]. Studying these special surfaces has helped in theorizing the basis of their desirable wettability with the ultimate goal of designing new surfaces with controllable wettability [35], [36].

In the 19th century, great emphasis was put on surface chemistry to explain this behaviour as was demonstrated by Young's model of wettability that explains the intrinsic hydrophilicity (high energy) and hydrophobicity (low energy) of a surface based on intermolecular forces. However, surface chemistry alone was not adequate to explain the phenomenon of superhydrophobicity possessed by surfaces with contact angles higher than 120°. The Wenzel and Cassie Baxter models appeared in the first half of the 20th century highlighting the importance of surface morphology on wetting behaviour. However, our understanding of these surfaces was only as good as the resolution afforded by our instrumentation.

The introduction of the first commercial scanning electron microscopes (SEMs) in 1965 opened a new world of possibilities by dramatically improving the resolution at which we could inspect the biological surfaces showing extreme wettability [37]. A wealth of such data has been collected since the 1960's [38].

Barthlott and Neinhuis in 1997 were the first to correlate the hydrophobicity demonstrated by natural surfaces to their topology. Their investigation revealed that special wettability was linked to the presence of microstructures in the form of micro-scale papillae and epicuticular wax present on the surface [5], [38].

At the start of the 21st century, the presence of smaller branch-like nano-scale structures on top of the micro-papillae revealed that special wetting behaviours were a consequence of a highly organized, multiscale hierarchical structure [39], [40]. The rose petal also showed extended nubs covered with waxy nanocrystals under an electron microscope. It is now widely understood that nanoscale roughness is essential in the fabrication of superhydrophobic surfaces with very high contact angles and low sliding angles that results in water-repellency and associated self-cleaning. Furthermore, the arrangement and orientation of these multiscale structures influence how water droplets tend to move on these surfaces e.g. in the case of anisotropic dewetting of the rice plant. These observations from the natural world provided guidelines for the synthesis of new materials possessing controllable wettability [40], [41].

2.2 Fabrication of MEWP

Many different methodologies have been employed by researchers over the years to fabricate materials with programmable wettability. Different methods utilize a combination of the same two conventional approaches:

- Roughening the surface of intrinsically hydrophobic/low energy materials (SCA>90º)
- Modifying an already rough surface with low surface energy (or hydrophobic) molecules (such as long chain fatty acids, organic silanes particularly fluoroalkyl silanes [40], thiols and azides) [42]

In some methodologies, fillers and nanoparticles are used to enhance surface roughening.

A brief overview of some of these strategies is as follows:

- Plasma treatment followed by deposition of a low-surface-energy layer [43]
- Casting on microporous templates to create patterned array structures [44]
- The layer-by-layer method first introduced in 1991 by G. Decher [45] through which it is possible to fabricate multilayer assemblies using a large number of building blocks as done by Zhao et al. [46] and Zhai et al. [47]. These include water-soluble polyelectrolytes, polymers bearing hydrogen donors and acceptors, biomacromolecules such as enzymes and DNA, colloid particles, oligo-charged dyes, and so on [46].
- Electrochemical synthesis including electrochemical deposition of gold, silver, zinc oxide and copper etc. on anodized materials [48], electrochemical polymerization on electrodes followed by deposition of low energy materials [49], galvanic cell reactions by which metallic nanoparticles can be deposited on substrates, [50] and roughening by anodic oxidation of metal plates for the deposition of low energy molecules [51].
- Sol-gel which involves polymerization of a colloidal sol through hydrolysis and polycondensation reactions resulting in the development of a 3D porous network within a wet, gel-like structure. Upon drying the gel incorporates any lingering particles into its network [52], [53], [54].
- Electrospinning to fabricate nanostructured ultra-thin fibers, denoted as electrospun nanofibers (ENFs) from a wide range of polymeric materials. These ENF's can be deposited on any surface to create nanoscale roughness necessary for superhydrophobicity [55]. Ma et al. prepared superhydrophobic block copolymer fibers through this electrospinning technique [56].

- Lithography, a top-to-bottom approach involving printing of natural surfaces and transferring them onto substrates [57]
- Chemical etching creates surface roughening because of the dislocation defects found in crystalline metals being more prone to dissolution. This is followed by surface fluorination which lowers the energy of the surface [58]
- 3D printing provides a new way to topographically engineer surfaces. A single-step 3D printing process can be utilized to produce an ordered mesh by using an ink with low surface energy molecules already mixed into it [59], [60]. Yang et al. also describe a novel additive manufacturing process called *immersed surface accumulation based 3D printing* based on the accumulation of material along the movement of a light guide tool inside a photocurable resin. Consequently, an inserted object can pick up photocured resin as the light probe moves, fabricating multiscale structures on its surface to achieve enhanced hydrophobicity [61]

The strategies mentioned above have produced many useful MEWP that find application in a multitude of different fields. However, methods and materials designed for the conservation of heritage must meet specific criteria that dramatically narrows down the list of applicable strategies. A method developed for the conservation of stone-built cultural heritage must (i) be suitable for the treatment of very large surfaces under normal ambient conditions, (ii) not include the use of expensive materials due to the scale of application, and (iii) be flexible for the treatment of various stone types.

Furthermore, the materials being utilized must fulfil some requirements such as no colour and/or reflectance changes, a significant reduction in water penetration, negligible changes in breathability, good adhesion, mechanical and physical durability, transparency and no formation

of harmful by-products. Finally, the intentional easy removal of the protective material, whenever necessary, is a desirable property to aspire towards despite being difficult to achieve on a porous substrate such as stone.

For this purpose, what follows is a review of the materials and methods tailored for use in the field of cultural heritage conservation, particularly those designed for the protection of stone-built heritage [62].

2.3 MEWP for the protection of stone heritage

The history of surface treatment conducted on stone objects dates back to ancient Greek and Roman periods and presumably even further back in history, when natural materials such as oils and waxes were used for protection and polishing purposes [63], [64]. The extensive use of polymeric substances in conservation is due to their ability to form protective outer layers and control the transport of different fluids from the surface to the monument's interior [65]. Traditionally polymeric resins, acrylic and vinyl polymers, organo-silicone compounds and fluorinated film-forming agents have been used for this purpose [66,] [67], [68].

Among the many hydrophobizing commercial resins, film-forming alkoxy-silanes/siloxanes and their composites have shown the most promising results. Unlike acrylic polymers, siloxanes do not necessitate the use of toxic organic solvents and show much less sensitivity towards colour changes under UV radiation [69]. Fermo et al. studied the nature of the resulting stone-resin surface interaction, by depositing a commercial siloxane, Alpha®SI30, on marble, limestone and dolomite substrates. A multi-analytical approach revealed that a homogeneous crack-free resin layer was formed on the stone surface. However, the coating was found to be too thin to mask the contribution from the roughness of the substrate [65]. Consequently, the protection offered by the

pure polysiloxane was limited by the nature of the substrate as the smooth and thin film simply followed the roughness and porosity of the underlying surface. Due to this, pure polymer systems typically only impart weak hydrophobicity to the substrate [66], [67], [68].

Lettieri et al. tested the performance of a siloxane in different concentrations on a highly porous calcarenite stone called "Lecce stone" [70]. Despite the high porosity of the substrate, a high concentration of siloxane resulted in cracking and a consequent loss of protection against water uptake by capillarity. Such cracking is frequently exhibited by products that polymerise by a sol-gel route and is attributed to shrinkage that occurs during the drying phase [70]. This highlights a limitation in the extent to which we can maximize hydrophobization simply by increasing the concentration of the polymer. Therefore, the hydrophobicity imparted to stone by polymer systems needs to be enhanced through modification.

As discussed earlier, two major factors control the wettability of a surface: surface energy and surface roughness. To develop materials with extreme wetting properties (SCA > 150◦ accompanied by low CAH) both factors need tuning to produce a nanostructured surface covered by a low-surface energy material. In the last two decades, two main approaches have been developed to produce such MEWPs [62].

The most popular approach used is to disperse inorganic nanoparticles in a polymer solution, or preferably in a polymer precursor solution composed of silanes and siloxanes. Inorganic nanoparticles (such as those of Ag, SiO_2, TiO_2, ZnO, ferrites and other metal oxides) possess many desirable physicochemical properties including high cohesion due to large surface area, high depth of penetration due to nano dimensions and good optical properties. Moreover, the photocatalytic activity of TiO_2 and ZnO nanoparticles can impart self-cleaning properties to the nanocomposite

material [20]. A highly rough surface is produced when the nanoparticle dispersion is deposited on stone often without the need for low-surface energy materials because NPs tend to form nanostructured clusters within the polymer matrix [62].

Manoudis et al. pioneered this approach in 2007 [72]. The group used SiO_2 NP's (7nm diameter) to roughen the surface of Poly(methyl methacrylate), PMMA, and perfluoropolyether, PFPE, followed by their application on marble and calcium carbonate substrates. These nanocomposites successfully imparted superhydrophobicity to stone, transforming the static contact angles of the pure polymer systems from 108° to 157°±3° and 112° to 162°±2° for PMMA and PFPE respectively. PMMA is an intrinsically hydrophilic polymer that was successfully made superhydrophobic through surface roughening, pointing at the great potential of the nanoparticle treatment to transform surfaces [72].

The pioneering methodology involved the dispersion of oxide nanoparticles in an alkoxy-silane/siloxane dissolved in organic solvent. The dispersion was then applied by spraying on the target substrate followed by annealing under vacuum at 40°C to remove the solvent. During this process, the alkoxy silane/siloxane undergoes a sol-gel process resulting in a continuous poly(alkyl siloxane) material of very high viscosity i.e. enriched with NPs [71]. The simplicity of the preparation and deposition methods and the price and availability of the materials made this approach promising for use in the protection of stone monuments [72]. Since then, the methodology has been improved and applied on various types of substrates offering promising results.

Manoudis et al. also investigated the role of nanoparticle concentration on the SCA and CAH using PMMA and a commercial poly(alkyl siloxane) called Rhodorsil 224, treated with SiO_2 NP's [24].

It was found that the SCA of surfaces treated with dilute dispersions (<1% w/v) increased rapidly with increase in nanoparticle concentration until it reached a maximum value. Further increase in particle concentration had no effect on the SCA.

The CAH, however, displayed a more complicated behaviour by first increasing with increase in particle concentration and then decreasing at higher particle concentrations [24]. Above 1% w/v the films showed comparable (and low) hysteresis values. This behaviour was explained through a mixed regime using data from atomic force microscopy (AFM) and SEM imaging. At high particle concentration the Cassie-Baxter model explains the low hysteresis due to the composite wetting phenomenon. However, at lower particle concentrations there are large areas on the surface that are still smooth and the water droplets falling on these smooth areas behave like Wenzel drops. This explains the high hysteresis associated with the pinned "sticky" state at low concentrations. Since the smooth areas quickly get populated with aggregates as particle concentration increases, the shift into the low hysteresis associated with the Cassie-Baxter conformation can be observed. This behaviour resembles the effect of roughness on wax, Teflon and PDMA surfaces and has been reproduced in other works as well [43], [73], [74], [75], [76].

Another study by the same group confirmed that the nano-scale of the particles was essential in creating extreme wetting behaviour as micro-scale particles following the same methodology failed to produce superhydrophobic coatings [77]. This result validates our assumption that the surface topography responsible for extreme wetting behaviour is directly reproduced by the dimensions of nanoparticle aggregates [77].

Manoudis et al. also demonstrated that the choice of substrate, type of nanoparticle and choice of polysiloxane had very little impact on the wettability of the nanocomposite films [78]. This implied

that many different combinations of polysiloxanes and metal oxide nanoparticles should be able to impart superhydrophobicity to stone; thereby greatly expanding the versatility of these water-repellent polysiloxane nanocomposites both in the materials used to synthesize them and the types of surfaces that could be protected by them [78].

De Ferri et al. tested the performance of a polysiloxane nanocomposite on granite, sandstone and limestone [79]. The coatings aged well, maintaining a high SCA of 150° even after four months of exposure to atmospheric conditions for all stone types. However, protection from water absorption by capillary action was only promising in the case of granite. On sandstone and limestone the nanocomposite did not offer sufficient protection after prolonged contact with water due to film cracking [79]. To make these nanocomposites applicable in real-world contexts, it was necessary to incorporate crack-resistance into their design.

As exemplified by de Ferrie et al. polymeric water repellent treatments applied on porous carbonate substrates often provide only limited protection from water absorption by capillarity despite showing very high initial SCA measurements. This can be caused by limited chemical bonding between the polymer and the stone, differences in the thermal expansion coefficients between the two components, as well as a low degree of pore surface modification [80]. A more persistent modification is expected if the hydrophobizing agent also carries functional groups that can bind strongly to calcareous stone surface e.g. phosphate, phosphonate or carboxylic groups. The use of nano-scale surfactants can accomplish this by improving diffusion through the porous stone matrix and promoting better binding between the organic polymer and the inorganic substrate.

In 2013, Facio et al. achieved this by adding a surfactant, n-octylamine, to the mixture that catalyzes the sol-gel transition while also preventing crack formation [81]. In this way they were able to synthesize a crack resistant water repellent nanocomposite. Alongside Chatzigrigoriou et al., they also introduced an application-oriented improvement in methodology as both groups used a low-cost one-step synthesis offering great potential for large-scale application [82]. The improved methodology eliminated the use of volatile organic compounds and the need for heat during the annealing step [81]. Chatzigrigoriou et al. dispersed silica nanoparticles in a commercial aqueous mixture of silanes and siloxanes through vigorous stirring. The resultant waterborne product was applied though brush application on marble, sandstone, mortar, wood, cotton and ceramic substrates and cured at ambient temperature and humidity. The treatment produced high SCA (>160^{o}) and low SA (< 5^{o}) with an improved methodology that was both environment and conservator friendly [82].

An alternative method to synthesize such materials is to polymerize precursors of siloxanes/silanes. Coricione et al. explored a photopolymerization technique that involved "dual-curing" of a mixture of methacrylate-siloxane-based monomers to produce an O-I hybrid coatings with embedded SiO_2 nanoparticles [83]. The mixture was first photo-polymerized with UV radiation and then heated at 140^{o} to complete a thermal stage of the sol-gel process that was responsible for the formation of SiO_2 NP's. SEM analysis of the cured film confirmed that the silica NPs were incorporated into the methacrylic-siloxane matrix. The coatings were tested on a calcareous stone and showed good hardness, extraordinary hydrophobicity and appropriate breathability while maintaining transparency [83].

In the last two decades, a growing interest was also seen in the production of superoleophobic surfaces corresponding to high oil contact angle (OCA) and an ability to repel oil. Such a material

could offer added protection from oil-based soiling agents such as spray paint. Anti-graffiti protection for heritage monuments could help reduce maintenance costs and minimize the need for restoration interventions. However, creating a superoleophobic surface is a challenging task, as it is more difficult to impede the wetting of low surface tension liquids, such as oil, compared to water. Luckily, many superoleophobic materials synthesized also show superhydrophobicity, exhibiting what is termed as superamphiphobicity or super-omniphobicity. This extreme wetting behaviour is highly desirable for the protection of stone monuments for virtually any kind of contaminating fluid.

Aslanidou et al. were successful in producing a superhydrophobic nanocomposite that also displayed superoleophobic behaviour and elaborated on the Cassie-Baxter to Wenzel transition in a series of stick-slip events during evapouration [84]. As mentioned in the previous section, the transition from a meta-stable Cassie-Baxter to a thermodynamically stable Wenzel state is commonly observed in MEWP and is particularly frequent for low surface tension liquids such as oil. This work contributed towards understanding the behaviour of low surface tension fluids on nanocomposite surfaces [84].

A superomniphobic coating was also prepared on silk substrates and the treatment was shown to be completely reversible under compressed liquid carbon dioxide [85]. And a similar superomniphobic, water and oil repellent material made from alkyl silane, organic fluoropolymer and silica nanoparticles was tested on marble and sandstone [86]. The coatings offered good protection against water penetration by capillarity and slightly reduced the breathability of the substrate with practically no effect on stone optics. However, the coatings showed a severe transition of wettability, from superhydrophobicity to superhydrophilicity, upon extreme thermal treatment as hydrophobic (methyl) groups were replaced by hydrophilic (hydroxyl) groups in the

FT-IR spectra [86]. This adds to the complexity of these types of extreme wetting nanocomposites in real-world applications.

In 2018 Lettieri et al. tested the ability of an experimental material, nanoF, consisting of a fluorine resin containing SiO_2 nanoparticles to impart hydrophobicity and oleophobicity to calcareous stone [87]. Its performance was compared to two commercial materials, one fluorine-based (Fluoline PE) and the other silicon-based (Kimistone DEFENDER). The new material had better optical properties compared to either of the commercial products, and also showed an unexpected improvement in vapour permeability possibly due to high hydrophobicity of the pore walls inside the stone brought about by the application of the nano-filled coating [87]. However, reduction in water absorption by capillarity was not significant for all despite all treatments showing low wettability [87]. In another related study on the same nanoF material, the treatment was tested for potential anti-graffiti action due to its oleophobicity [88]. It was found to offer protection from artificially simulated pancreatin (pigeon excrement), but the anti-graffiti protection efficacy was found to depend more on the staining agent and cleaning procedure than the surface treatment. However, the nanoF product did fulfill the sustainability criteria in the development of conservation materials, as it offered protection comparable to commercial products in much smaller amounts [88].

In addition to the damage caused by water and graffiti, environmental pollutants in urban areas also pose a serious threat to historic monuments and often work in unison with water. As a result, efforts have also been made to synthesize materials capable of degrading environmental contaminants by exploiting the photocatalytic properties of different semiconductor metal oxides [89]. Among these, TiO_2 is the most widely used due to its low cost, safety, chemical stability and high photocatalytic efficiency [90], [91]. The development of photocatalytic products active in de-

soiling is a possible way to limit soiling damage and to reduce the frequency of costly cleaning operations [92].

Unfortunately, commercial nano-TiO_2 dispersions are known to produce non-homogenous whitish films and do not perform well under solar radiation as they contain a UV component of less than 5%. To meet this need, Gherardi et al. prepared nano-TiO_2 based dispersions that were photo-active under solar irradiation due to the presence of benzyl alcohol molecules involved in the non-aqueous synthesis [93]. It was also found that the photocatalytic performance of the TiO_2 nanocomposites was highly dependent on the porosity of the stone substrate as well as the solvent used to create the dispersion. A water-based treatment gave optimal results on porous limestone and a 2-propanol based treatment worked well when it came to compact marble [94].

Cappelletti et al. found that hybrid coatings of TiO_2 and silane were more effective in reducing salt formation compared to the pure resin [95]. Kapridaki and Maravelaki-Kalaitzaki and D'Orazio and Grippo had also designed transparent and hydrophobic TiO_2-based hybrid coatings that conferred antibacterial activity and self-cleaning behaviour to stone substrate thus preventing biofilm growth and pollutant absorption [96], [97]. The choice of binder and its effect on the photocatalytic efficiency and hydrophobicity of nano-TiO_2 coatings was investigated by La Russa et al. [98]. They demonstrated that the performance of the coating was related to the depth of penetration into the pore structure. Greater depth of penetration ensured both durability and hydrophobicity [98].

In more recent studies, Chatzigrigoriou et al. have utilized $Ca(OH)_2$ nanoparticles to create new polysiloxane nanocomposites that impart superhydrophobicity to stone with an excellent chemical compatibility with limestone and limestone-like rocks (marble, travertine). The nanocomposites

provided good protection against water penetration by capillarity with only a small effect on the colour of the stone [99].

The nanoparticle approach has yielded many interesting MEWP with great versatility and applicability on a range of substrates offering protection from pigeon excrement and environmental pollutants. It also shows excellent results when it comes to minimal colour variation, as most nanoparticles are whitish. So much so, that a polymer-NPs composite has also been reported to induce less colour change to sandstone than the corresponding pure polymer did [86].

However, there are some concerns and limitations. The stability of the hydrophobic character of the self-cleaning nanocomposites when exposed to prolonged UV-radiation has been questioned and not enough is known about the potential health and environmental risks associated with the use of nanoparticles [100].

Moreover, many nanocomposites with very high SCA have not shown proportional protection from water. Some superhydrophobic and hydrophobic surfaces have been shown to offer the same protection from water absorption by capillarity. Interestingly, some superhydrophilic materials have also offered protection against water absorption provided a hydrophobic component is present in the material [101]. Consequently, the actual performance of these nanocomposites must not be inferred from their very high WCAs and OCAs alone as this is not a reliable measure of water repellency. CAH and SA parameters are necessary but they are often excluded from literature [102].

A second strategy to develop superhydrophobic and highly hydrophobic materials for the protection of stone includes the use of sols, solutions or emulsions which contain low surface energy materials. Many such functionalized polyolefins have been synthesized over the years.

Tetraethoxysilane (TEOS) is a material that has been widely used to produce organic-inorganic (O-I) hybrid materials for stone preservation. TEOS is one of the most used stone consolidants, [103] whose effectiveness derives from hydrolysis-condensation reactions that lead to the formation of amorphous silica inside stone pores [71], [104], [105], [106]. The compatibility of the deposited silica gel with silicate substrates guarantees high durability on silicate stone [71]. However, its effectiveness is known to depend on the presence of quartzitic fractions inside the substrate. Consequently, TEOS-based consolidants have a tendency to crack during drying when applied to carbonate stone and are notorious for imparting only temporary hydrophobicity [103]. As we have seen, the use of surfactant has been widely adopted to improve crack-resistance and durability of conservation materials. Mosquera et al. synthesized a new O-I hybrid nanomaterial via sol-gel through the co-condensation of tetraethoxysilane (TEOS) and hydroxyl-terminated polydimethylsiloxane (PDMS-OH) in the presence of a non-ionic surfactant. The hybrid material was shown to improve the mechanical durability of the stone and create hydrophobicity with no associated negative effects on the treated stone. The material was also crack resistant due to both the PDMS and the surfactant. The former enhanced flexibility and shrinkage and the latter reduced surface tension of the solvent thereby facilitating homogenous co-condensation with regular pore sizes [107].

Further efforts to create crack-free TEOS materials resulted in an O-I hybrid xerogel made by Dan Li et al. PDMS-OH was used as an additive to TEOS with di-n-butyltin dilaurate (DBTL) serving as the catalyst. The DBTL was found to decrease gelling time, thereby increasing efficiency and

the xerogel's cracking was improved by the addition of PDMS-OH. Moreover, it is known that the addition of colloidal silica particles to TEOS-based consolidants shows a significant reduction in fracture percentage and prevents cracking of the gel network during the drying phase [108], [109]. Therefore, a hybrid TEOS-SiO_2-PDMS-OH solution was applied to limestone that increased both surface roughness and associated hydrophobicity (up to 97°) without any colour changes [110].

Later, Luo et al. investigated the possible use of nano-hydroxyapatite (n-HA) as a new inorganic consolidant [111]. The composites were prepared by the co-condensation of TEOS and PDMS-OH in the presence of n-HA. The TEOS/PDMS/n-HA material imparted enhanced hydrophobicity to the stone without compromising vapour transport. The improved hydrophobicity was achieved by the reduction of surface tension by PDMS and the increase of surface roughness by n-HA. The n-HA was also reported to effectively improve mechanical properties, crack-resistance, and weathering resistance without any colour changes to the stone [111].

Liu et al. created a similar composite for sandstone protection based on TEOS, PDMS-OH and a surfactant i.e. cetyl trimethyl ammonium bromide (CTAB) [112]. The CTAB created protrusions with the micro and nano-scale structure and prevented cracking during the drying process. The TEOS-PDMS-OH/CTAB coating improved the sandstone's ability to resist acid and salt crystallization weathering significantly [112].

A special class of surfactants called fluorocarbons/fluorosurfactants are known to possess an exceptional ability to lower surface tension of polymer systems even when added in very low concentrations. These fluorinated molecules impart enhanced hydrophobicity and the polar groups of the surfactant facilitate stronger attachment to the stone substrate [113]. Perfluorooctanoic acid

(PFOA) and perfluorooctane sulfonate (PFOS) are two fluorosurfactants that are typically associated with fluoropolymers. Their chemical structure can be seen in figures 5 and 6.

Figure 5: Chemical structure of perfluorooctanoic acid (PFOA)

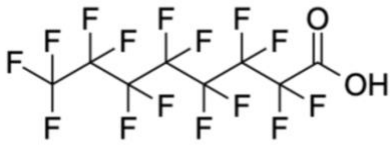

Figure 6: Chemical structure of perfluorooctane sulfonate (PFOS)

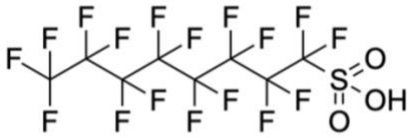

However, in recent years, these C8 (eight-carbon) fluorocarbon products have been shown to be environmentally persistent and potentially hazardous in nature. In response to environmental concerns, C8 FCs can be replaced by short-chain fluorocarbons to create ecofriendly fluorinated polysiloxanes (FPS) like the ones utilized by Ugur in 2014 [116].

These fluorinated polysiloxanes (FPS) can be applied at room temperature without any need for special equipment. Additionally, Ugur proposes that unlike film-forming coatings e.g., acrylic and epoxy resins, these water repellents do not seal the pores of the stone surface thereby disturbing the breathability of the stone. Instead, Ugur's FPS are proposed to form a thin layer on the pore walls as can be visualized in figure 7. It should be noted that numerous studies on siloxanes have

shown that they do not affect vapour permeability to a large extent. However, the same cannot be said for acrylics.

Figure 7: Stone surface with a) FPS impregnation b) filled pores c) film-forming sealant

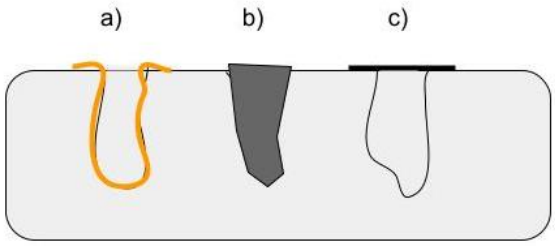

Ugur modified two porous stones, limestone, and tuff, with a C6 fluoropolymer producing a byproduct supposedly 40 times less bio-accumulative than PFOA. Based on the anticipated low water solubility, it had very low mobility in soils making it an eco-friendly chemical [115], [116]. The general schemes for the organo-silicates and C6 fluorocarbons used are shown in figures 8 and 9 respectively.

Figure 8: General scheme for the organo-silicates

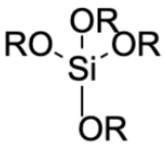

Figure 9: Scheme for C6 fluorocarbons

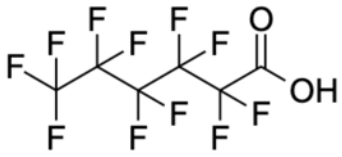

Ugur's FPS treatment effectively imparted hydrophobicity to both porous stones without any colour variation and maintained this hydrophobicity, up to a certain degree, even when exposed to extreme temperatures [116].

Kronlund et al. in 2015 proposed a strategy of total immersion to maximize the hydrophobicity achieved on marble through products containing fluorosurfactants/fluorinated polymers [117]. The contact angle measurements for six different products showed the SCA transformed from 64 ± 3° for untreated marble to ~100° or higher, implying that the outermost surface was successfully hydrophobized. Mechanical grinding and capillary absorption measurements indicated functionality of the hydrophobic molecules up to a depth of 2 mm with no reduction in breathability. One of the products maintained 0% water uptake by capillarity for up to 72 hours of UV irradiation indicating that the total immersion strategy facilitates deep penetration resulting in protection from water uptake even when the outermost layers are abraded [117]. Fluorinated oligomers have also been tested by Cao et al. [118].

Although this second approach benefits from the absence of NPs in the recipe to achieve hydrophobicity, the fluorinated compounds frequently used as low-surface energy agents are hazardous as well and possess high environmental stability and mobility [119]. Since the highest SCA achieved on a smooth surface is that of Teflon at 120º it is clear that this approach works best

on substrates that are already roughened. This makes this approach best used in combination with other methods.

This body of work utilizes the improved methodology described in the review paper by Karapanagiotis and Manoudis [151] to develop superhydrophobic and superamphiphobic nanocomposite coatings from two commercially available polysiloxanes, a C6 fluorocarbon polymer and SiO_2 NP's. The work follows the characterization of the novel nanocomposites' wettability, mechanical strength and response to artificial aging.

3 Materials

The two novel superhydrophobic coatings characterized in this work were produced by dispersing SiO_2 nanoparticles in two commercial organo-functionalized silanes by Evonik called Dynasylan® SIVO 121 and Protectosil SC®. The coatings were deposited on marble substrates to test their protection of the stone from water penetration and other related parameters.

3.1 Marble

Marble is a metamorphic rock formed from limestone under extreme temperatures. The parent rock consists of carbonate minerals i.e. calcite and dolomite. Under extreme temperature and pressure these minerals grow larger and fuse together to form marble. The different colours and patterns of marble depend upon the impurities present during rock formation. Marble has been valued for its durability and aesthetic appeal since ancient times. Our choice of substrate is based on the fact that a large volume of the world's stone heritage utilizes this precious natural stone [120].

The marble used in our experiments originated from Serres, Northern Greece, not far from the Drama-Kavala-Thassos region that is famous for its ancient marble quarries [121]. The marble used showed a compressive strength of ~150 MPa, a porosity of 0.5% and a specific gravity of 2.8 based on the RILEM CPC 11.3:1984 test method reported by Dr. Tsiridis.

3.2 Dynasylan® SIVO 121

Dynasylan® SIVO 121 is a commercial wood surface impregnation agent that protects wood substrates from degradation caused by exposure to water and oils by imparting hydrophobic and oleophobic properties to these substrates. Our research group was interested in testing the product's performance on a mineral substrate.

Evonik reports Dynasylan® SIVO 121 to be a water-borne silane system that is nearly VOC-free and contains multiple fluoroalkyl functional groups. VOC's are gasses emitted into the air from some products and processes that are toxic when inhaled and known to be carcinogenic. They can also react with gasses in the air to form other air pollutants [122]. Therefore, it is an important environmental consideration to try to eliminate the use of VOC and organic solvents. This product meets this criteria making it a safe and environmentally friendly choice.

3.3 Protectosil® SC

The environmentally friendly Protectosil® SC products are valued for their ability to impart hydrophobicity and oleophobicity to any mineral surface upon application and provide ideal protection for porous substrates such as sandstone and brick masonry, concrete, marble, or granite. This product is a corrosion inhibitor that penetrates the substrate deeply and does not allow the ingress of water and water-soluble pollutants. The deep penetration in the substrate implies that its protection should not be affected by abrasive load or exposure to ultraviolet radiation from the sun.

Herein, the potential of creating a superhydrophobic nanocomposite from this product through the introduction of nanoparticles has been explored [123].

3.4 Fluoropolymer

The fluoropolymer additive used has a commercial name Daikin Unidyne TG 5601 and is a cationic C6 fluorocarbon polymer. As discussed previously, C6 fluoropolymers are much more environmentally friendly than their C8 counterparts [115].

3.5 SiO_2 nanoparticles

The SiO_2 NPs with diameter of 7 nm were selected as they have shown good results in previous studies. These were commercially acquired in fumed powder state from Sigma Aldrich.

4 Background information

This chapter details the work done prior to this research in preparing and depositing the novel coatings that were later characterized in the methodology, results and discussion chapters. It also includes a brief reasoning behind the shortlisted treatments that were tested alongside their initial static contact angles and colour measurements.

4.1 Preparation and deposition of the coatings

For the first treatment group, Dynasylan® Sivo 121 was diluted to a 20% w/w aqueous solution labelled D. 1% w/w SiO_2 nanoparticles (fumed powder, Aldrich, 7nm) were introduced into D through vigorous mixing for 20 minutes. The dispersion labelled D/S was immediately sprayed onto marble. A 2% w/w SiO_2 nanoparticle (fumed powder, Aldrich, 7nm) variant called D/2S was

also prepared. To further boost the hydrophobic/oleophobic character of the nanocomposite dispersion, a small quantity of fluoropolymer (C6 fluorocarbon polymer, cationic) was introduced into the D/S dispersion to create the D/S/F treatment.

For the second treatment group, an aqueous solution was prepared with Protectosil® SC and fluoropolymer (C6 fluorocarbon polymer, cationic) in the ratio 6:1 labeled 6P/1F. Next, a nanocomposite was prepared by vigorous stirring of 2% w/w SiO_2 nanoparticles (fumed powder, Aldrich, 7nm) into the 6P/1F solution for 20 minutes. This was followed by immediate deposition through spraying onto the marble substrate. This treatment was labelled 6/F/2S. The different coatings with their corresponding labels are summarized in table 1. Table 2 goes on to list the contact angle measurements for each of these coatings across the Dynasylan and Protectosil groups.

Samples were prepared by spraying 0.08 g of each treatment per cm^2 of marble substrate followed by drying at 60^oC for 1 hour to enable curing through the sol-gel process and to remove excess solvent.

Table 1: List of treatment types and their labels

Treatment Type	Label
20% w/w aq. sol of Dynasylan®	D
D + 1% w/w SiO_2 NPs	D/S
D + 2% w/w SiO_2 NPs	D/2S
D + 1% w/w SiO_2 NPs + fluoropolymer	D/S/F
D + 2% w/w SiO_2 NPs + fluoropolymer	D/2S/F
Aq. sol of Protectosil® SC and fluoropolymer (6:1)	6P/1F
6P/1F + 2% w/w fluoropolymer	6P/1F/2S

A preliminary comparison was done between treatment variants to optimize the nanoparticle concentration and siloxane to fluoropolymer ratios in the coatings selected for further testing, listed in table 1.

The effect of nanoparticle concentration on the Dynasylan nanocomposites was revealed in the SEM images in figures 10a, 10b and 10c [153]. The surface of treatment D is smooth (figure 10a) and affected only by the roughness of the underlying marble substrate. The D/S nanocomposite surface (figure 10b) shows the presence of micro-clusters carrying nanostructures [24], [62]. Therefore, a two-length-scale hierarchical structure is formed on the D/S surface [24], [62] which is responsible for the large WCA and OCA associated with these coatings [153].

Figure 10: SEM images of marble with treatments (a) D, (b) D/S, (c) D/2S (d) D/S/F

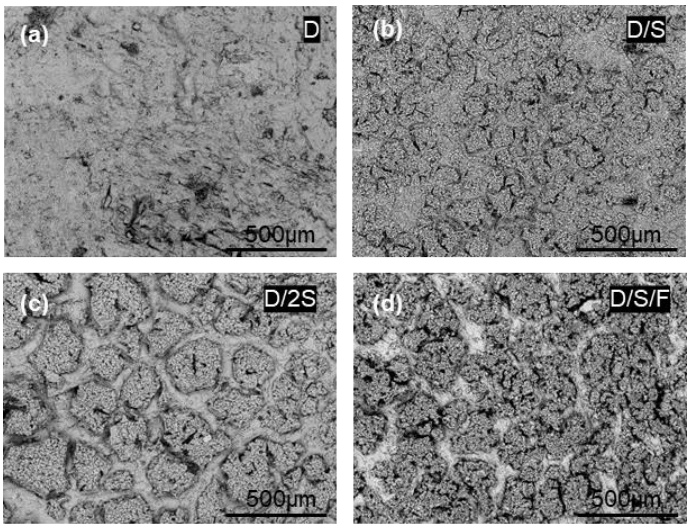

The SEM images of Figures 10b and 10c suggest negligible differences in the structures of the D/S and D/2S surfaces. The microclusters in the D/2S surface were only found to be slightly larger compared to the D/S surface. However, this small difference had no effect on the WCA which was practically the same for both D/S and D/2S surfaces. OCA, however, slightly increased with NP

concentration (Table 2) as low surface tension fluids are known to be more sensitive to slight changes in surface structure compared to high surface tension water droplets [102]. Overall, the structures of the D/S and D/2S surfaces were quite similar [153].

Previously published studies on the wetting properties of nanocomposites showed that beyond a specific critical value of NP concentration, the surface becomes saturated with hierarchical structures [78], [138]. Further increase of the NP concentration does not have a significant impact on the surface structure and the resulting WCA of the composite material [24], [62], [78], [138]. The critical value of the NP concentration depends on the type of the polymer and nanoparticles used. SEM images of figures 10b and 10c suggest that for the composite studied herein, the 1% w/w NP concentration is adequate to reach the saturation point, as no major difference is observed between the structures of the D/S and D/2S surfaces and their corresponding WCAs.

Taking into consideration that (i) the wettabilities of the D/S and D/2S coatings are similar and (ii) the increasing concern about the potential health and environmental risks associated with the use of NPs [100], [139], the low NP concentration of 1% w/w was selected to prepare the fluorinated D/S/F coating [153]. Similarly, different ratios of Protectosil SC, fluoropolymer and SiO_2 nanoparticle concentration were tested, and the treatments mentioned in Table 1 were shortlisted based on the best combination of SCA and colour differences, as well as an effort to select conservative amounts of additive to meet sustainability criteria.

4.2 Contact angle measurements

Contact angle measurements categorized the level of hydrophobicity and oleophobicity imparted to stone by each of the treatments. Commercially available olive oil was used for OCA

measurements. Table 2 summarizes both the water contact angle (WCA) and the olive oil contact angle (OCA) for each of the shortlisted treatments measured by Dr. Manoudis.

Table 2: Summary of initial contact angle measurements for each treatment.

Treatment	Water Contact Angle (WCA) (°)		Olive Oil Contact Angle (OCA) (°)	
	Mean	Stand. Dev.	Mean	Stand. Dev.
Dynasylan®				
D	115.6	1.7	87.9	2.8
D/S	133.40	1.83	111.5	1.55
D/2S	132.53	1.7	123.4	5.95
D/F	129.5	1	118.9	1
D/S/F	160	1	137	2
D/2S/F	161	1	94*	4
Protectosil® SC				
6P/1F	130.7	1.2	103.4	5.7
6P/1F/2S	160.3	2.5	152.2	0.7

The D/S/F coating is superhydrophobic with a WCA=160° and the 6P/1F/2S coating displays superamphiphobicity with WCA= 160.3° and OCA=152.2° These two novel MEWP are central to the following research work.

4.3 Colorimetric measurements

Before proceeding to other tests, it was essential to first quantify the colour change across treated and untreated surfaces as coatings intended for use in the field of conservation must conform to a narrow range of permissible chromatic variation in the substrate after treatment. A portable point-

and-shoot PCE-CSM 4 from PCE Instruments, UK [126] was used for colour measurements (figure 11).

Figure 11: Instrument used for colour measurements

A global colour difference parameter, ΔE, was measured across bare and coated marble samples and derived from equation (6) from the CIE 1976 scale [99],

$$\Delta E^* = \sqrt{(L_t^* - L_u^*)^2 + (a_t^* - a_u^*)^2 + (b_t^* - b_u^*)^2} \qquad (6)$$

where L*, a* and b* correspond to the brightness, red–green component and yellow–blue component, respectively. The 't' and 'u' subscript refer to the treated and untreated samples respectively [99]. Three measurements per sample were taken and the average values were reported.

The samples gave promising colorimetric results with all coatings showing a colour difference corresponding to $\Delta E < 5$. This colour variation is invisible to the human eye and deemed acceptable according to Italian guidelines for materials to be used for the conservation of historic surfaces [134]. The colorimetric results for the Dynasylan and the Protectosil SC treatment groups are summarized in tables 3 and 4 respectively.

Table 3: Colorimetric measurements for the Dynasylan group

Treatment	ΔE*	stdev
D	0.82	0.37
D/S	2.00	0.46
D/2S	2.05	0.30
D/S/F	3.61	1.41
D/2S/F	4.41	1.87

Table 4: Colorimetric measurements for the Protectosil SC group

Treatment	ΔE*	stdev
P	3.72	0.52
6P/1F	1.3	0.3
6P/1F/2S	1.9	0.4

The addition of nanoparticles to create materials with extreme wetting properties has consistently shown excellent results regarding minimal colour variation due to their whitish colour. To the extent that, in the past, a polymer-NPs composite has been reported that induced less colour change to sandstone than the corresponding pure polymer did [86]. The results shown by the superamphiphobic Protectosil coating are similar as the pure polymer displays a larger chromatic variation than the nanocomposite corresponding to much smaller ΔE values.

5 Methodology

5.1 Contact angle measurements

The Krüss Mobile Surface Analyzer (MSA) was used to confirm the WCA right before experimentation was consistent with that measured right after sample preparation. SCA was measured at three random points on the specimen, as shown in figure 12, and mean values were reported.

Figure 12: Krüss Mobile Surface Analyzer (MSA)

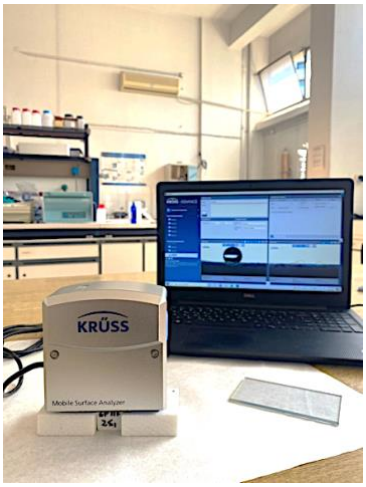

5.2 Water absorption by capillary action test

The treatments' ability to reduce water absorption by capillarity was evaluated using a gravimetric sorption technique [127], based on the European standard EN-15801 [152]. The test was carried out using 5 x 5 x 2 cm test pieces with one 5 x 5 face coated with the treatment under analysis. Prior to the test, the lateral sides of the samples were sealed with a layer of Teflon tape followed by a layer of electrical insulation tape. This was done to eliminate any contribution in mass change

due to contact of water with the bare sides of the specimen. In optimization attempts, paraffin followed by electrical tape was tested as the sealant. It did not provide satisfactory insulation.

Figure 13: Optimization run to test water absorption by capillarity

The dry weighed stone blocks were placed with the treated side face-down on a filter paper pad (1 cm of Whatman paper, No. 4) fully drenched in distilled water. The sample was extracted after regular intervals, blotted to remove excess water, and weighed. The test was run for 48 hours in total to give the low porosity substrate plenty of time to saturate in water and for the water uptake to flatline. Alternatively, the test can also be discontinued when the difference between two consecutive weights becomes less than 1% of the mass of water absorbed by the specimen according to the standard consulted [152]. The Protectosil group was tested by Dr Manoudis following the same protocol except without the need to insulate the lateral sides of the specimens.

The percentage reduction in water absorption by capillarity was measured by comparing the mass of water absorbed by the treated versus untreated surface using equation (8),

$$\% RC = \frac{m_u - m_t}{m_u} \times 100 \qquad (8)$$

where, m_u and m_t correspond to total mass of water absorbed by untreated and treated marble specimen respectively [128], [129].

Four test pieces per treatment and two untreated test pieces were used in each experimental run.

5.3 Water vapour permeability test

The vapour permeability test, based on the European standard EN-15803 [155], operated off creating a vapour pressure gradient across the specimen, through wet or dry conditions, to check for any change in the breathability of treated stone.

Protocol One:

Squared sample blocks with dimensions of 2 x 2 x 2 cm were fixed with the treated face up on top of identical cylindrical PVC containers half filled with saturated aqueous potassium nitrate (KNO_3) solution. The KNO_3 solution was used to simulate 93-95% humidity and create high vapour pressure inside the cup to promote vapour flow through the stone. The specimen was secured on the PVC container with electrical tape, after which the assembly was wrapped in paraffin leaving only the treated face exposed to air. The container was then placed at a temperature of 20^{o}C in a humidity-controlled chamber (R.H. = 40%) and weighed every 24-hours. The percentage reduction in vapour permeability was measured by comparing the mass change associated with vapour loss for treated and untreated stone surfaces. This protocol showed very low breathability resulting in very small numbers that were unreliable and nonrepresentative; therefore, the protocol was revised.

Protocol Two:

In this protocol a wet cup method shown in figure 14 was followed with the PVC containers half-filled with distilled water and the climatic chamber kept at an elevated temperature to promote vapour flow [129]. The PVC containers were sealed with a layer of tac followed by paraffin to direct vapour flow through the stone and out from the treated face. The use of tac showed better insulation results than the electrical tape used previously. The containers were placed in a climatic chamber at 40 ± 0.5 °C, R.H. 15% and weighed every 24 hours.

Figure 14: Vapour permeability test setup

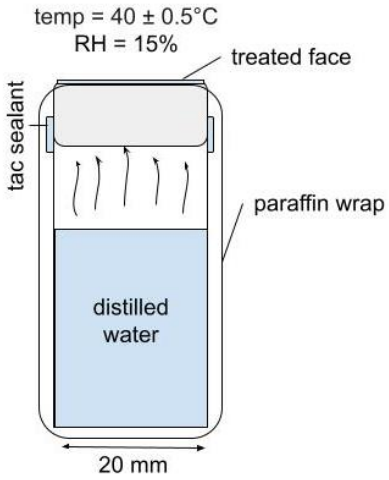

It was assumed that the vapour flow through the stone had reached a steady state when the variation between two consecutive 24 hour vapour losses, ΔM_{i-1} and ΔM_i, was less than 2% according to (9).

$$\frac{\Delta M_i - \Delta M_{i-1}}{\Delta M_i} \times 100 < 2\% \qquad (9)$$

Under constant vapour flow, the water vapour permeability was evaluated as the mass of water vapour passing through the surface unit in 24 hours [129]. The reduction in vapour permeability was calculate according to equation (10),

$$\%RVP = \frac{m_{uv} - m_{tv}}{m_{uv}} \times 100 \quad (10)$$

where m_{uv} and m_{tv} refer to the mass of vapour lost, in steady state, from the untreated/bare and treated/coated samples respectively [129]. Three test pieces per treatment and three untreated test pieces were set up.

5.4 Sandpaper abrasion test

The abrasion test was performed on 5 x 5 x 2 cm squared blocks, treated on one 5 x 5 cm face. The sample was placed face-down on the sandpaper (mesh 160) with a weight of 100 g placed on top (figure 15). Together with the weight of the sample this corresponded to a total pressure of about 0.92 kPa [153]. The sample was moved 10 cm along a ruler, rotated by 90° and moved for another 10 cm. This process is defined as one complete abrasion cycle which guarantees that the specimen is both longitudinally and transversally abraded in each cycle while maintaining movement in one direction [130], [131], [132].

Figure 15: Sandpaper abrasion test setup

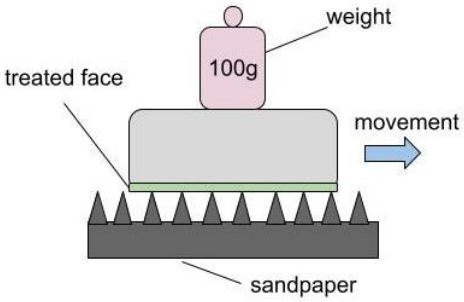

The samples were subjected to multiple cycles of abrasion, each followed by measurement of the contact angle. WCA was measured at five different points on the specimen. Two test pieces per treatment were tested.

5.5 Tape peeling test

The tape peeling test was applied using a Scotch Tape 600 (3M) according to the specifications described in ASTMD-3359 97. An adhesive tape (Scotch-600 tape) was glued to the treated 2 x 2 cm sample surface and firmly pressed down followed by a steady removal through peeling. This comprised one peeling cycle. WCA was measured in three different areas of the sample after each cycle [132]. Two test pieces per treatment were used.

5.6 Freeze-thaw test

The freeze-thaw test was applied on 2 x 2 x 2 cm samples treated in one face. The samples were subjected to freezing temperature of -22°C in a refrigerator for 15 minutes and then thawed inside a silica desiccator to room temperature [133]. WCA was measured in at least three different areas after each cycle. Two test pieces per treatment were used.

5.7 Acid/ rain simulation test

During the rain simulation test, the sample was placed about 50 cm away under a contraption (figure 16) that sprinkled water on it. A complete cycle of rain consisted of one liter of distilled water dropped on the sample over the course of roughly an hour. The sample was then dried at 60^{o}C in the oven for 10 mins to 2 hours. After the samples cooled down the WCA was measured at three random points on the surface.

Figure 16: (a) Rain water dispenser contraption (b) Artificial rain experimental set up

(a) 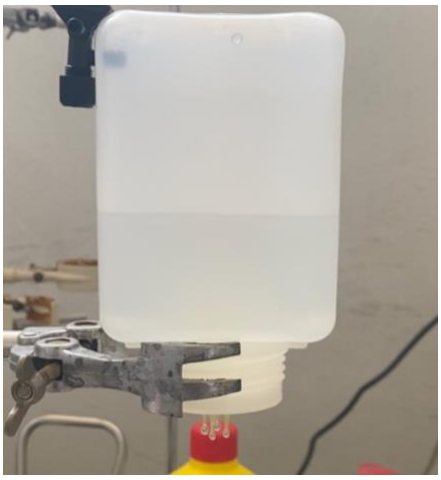 (b) 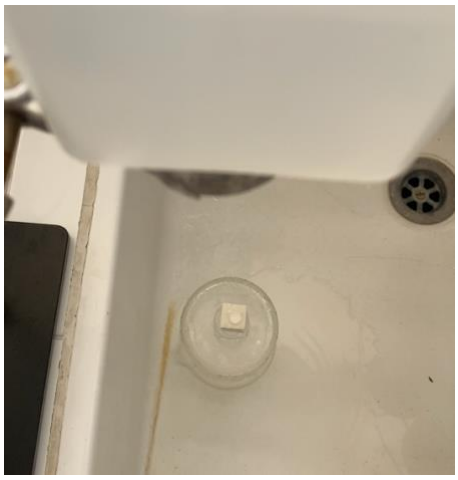

A variation of this test was set up to simulate acid rain. The water sprinkled on the samples in this test was acidified to a pH of 4.30. The rest of the protocol remained unchanged. Three samples were tested per treatment and more added for confirmation purposes.

5.8 Sand-grit erosion test

The sand-grit erosion test was performed on 2 x 2 x 2 cm squared blocks placed 0.4 m away at a 30° angle from the sand source (figure 17). Sand with a particle size < 230 microns was utilized A funnel dropped 50 g of this sand on the treated face of the specimen per cycle. WCA was measured in at least three different areas after each cycle until the contact angle dropped below 90°. One sample per treatment was tested.

Figure 17: (a) Sand-grit test experimental set up (b) Sand-grit erosion test in action

(a) 

(b) 

5.9 Accelerated UV-aging test

The artificial aging test was performed on 2 x 2 x 2 cm sample blocks placed 32 cm away from a UV source (Osram Dulux S Blue, 9W/78V, UVA 300-400 nm) inside a chamber (figure 18) for 60 days. The temperature of the chamber was kept at 27.7^{o}C and the radiation intensity on the sample was 1.064 W/m^2. The samples were inspected visually for colour variation and WCA was measured periodically in at least three different areas of the sample.

One test piece per treatment was tested.

Figure 18: (a) UV-aging set up (b) UV chamber in action

(a) 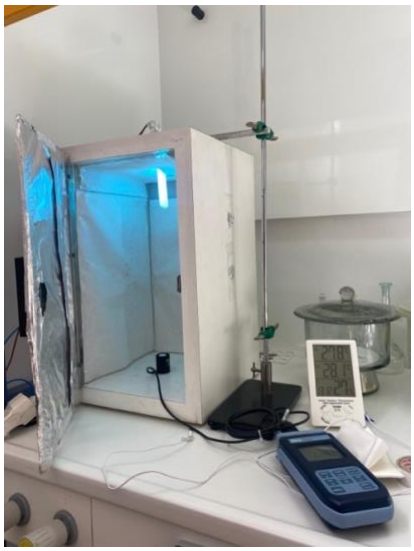

(b) 

6 Results and Discussion

Substantial time and effort were invested in developing and optimizing the test protocols used to obtain the following results. These protocols were adapted from standards, adopted from previous research, and optimized through trial runs. Six different runs of the vapour permeability test were used to optimize the protocol that was ultimately able to achieve steady vapour flow. Particularly, the sandpaper abrasion test was applied to coatings being developed for heritage application for the first time. The protocols and associated contraptions for the freeze-thaw, acid/rain simulation and sand erosion test were all developed entirely from scratch with the help of Dr. Tsiridis.

6.1 Water absorption by capillary action test

The mass of water absorbed from the capillary transport medium was directly recorded as a function of time. The amount of water absorbed by the specimen per unit area, Q_i (expressed in grams per square meter) at time t_i is calculated as follows,

$$Q_i = [(m_i - m_0)/A] \qquad (11)$$

According to simplified models for porous stones, the amount of water absorbed by capillarity should be proportional, through coefficients of stone porosity and water diffusivity, to the square root of contact time with the capillary transport medium up until saturation [135]. Figure 19 shows the progression of Q_i with the passage of time for the Dynasylan group. The shape of this graph shows a roughly linear trend for water uptake that eventually plateaus indicating that the stone has become saturated with water taken up from the capillary transport medium. This trend is typical for this test [4], [86].

Figure 19: Plot of Q against $t^{1/2}$ for the Dynasylan group

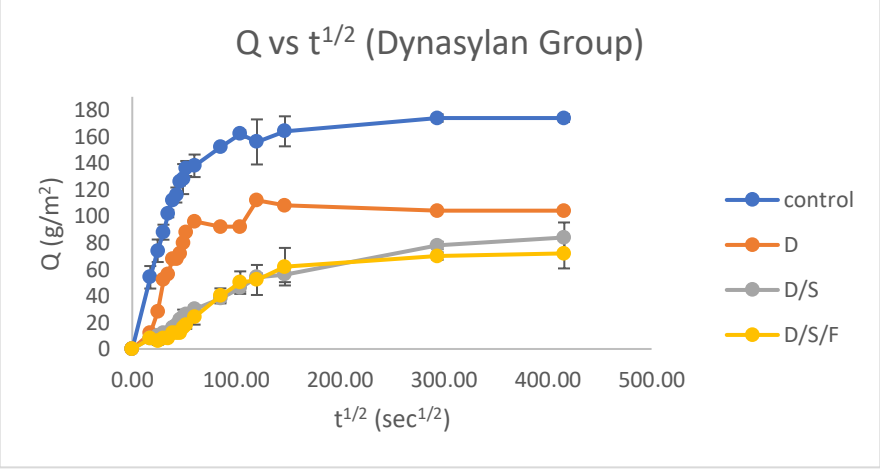

Intuitively, the maximum amount of water is absorbed by the bare marble samples. Treatment D decreases this quantity significantly and the nanocomposites show a further improvement in this reduction in water uptake by capillarity. To further investigate if there is any significant difference in the protection afforded by the two nanocomposites, D/S and D/S/F, the capillary absorption coefficients were approximated.

Despite marble's low porosity, Q_i could be linearly regressed against the square root of time up to saturation point. The slope of this regression gives an approximate water capillary absorption coefficient (AC) [152]. The AC values quantify the extent to which water is absorbed by each treatment. The accuracy of the coefficients depends on how well the linear regression fits the curve and is reflected by the associated R^2 values which should be 1 for a perfect fit. The linear regression of most samples corresponded to R^2 >0.9 implying a good fit. Figure 20 summarizes the AC values for the Dynasylan treatment group.

Figure 20: Approximate absorption coefficients for the Dynasylan treatment group

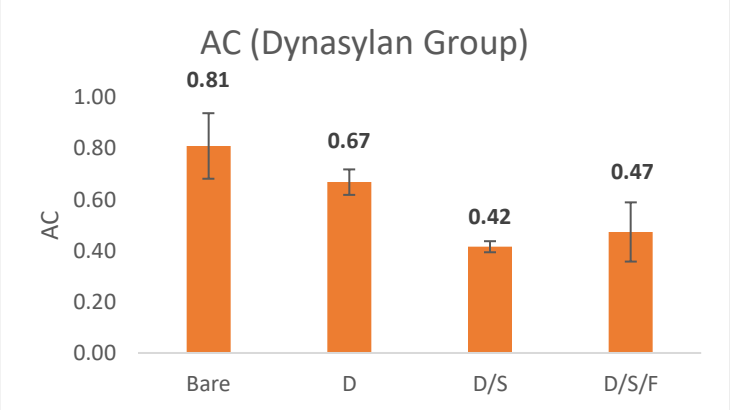

The difference in absorption coefficients for D/S and D/S/F fluctuate within the standard deviation indicating no significant difference in the protection afforded by the two nanocomposites. This is

a precedented result as many superhydrophobic and hydrophobic surfaces have been shown to offer comparable protection from water absorption by capillarity [101]. An enhancement in the SCA of the D/S/F treatment (WCA= 160°) compared to the D/S (WCA=133.40°), does not show a proportional enhancement in the protection against water penetration. However, it is important to note that this test alone is not a reliable criterion to judge the performance of a coating, as surfaces displaying superhydrophilicity have also been shown to inhibit water uptake by capillarity, provided at least one hydrophobic component is present [101]. Furthermore, durability tests affirmed that the D/S/F coating did offer improvement over the D/S coating, as the latter abraded much more readily than the former.

In more practical terms, the results are reported as the percentage reduction in water absorbed via capillary action (%RC), calculated using equation (8). In an ideal but unrealistic coating this reduction in water uptake should be 100% indicating that it is a perfect sealant whose application eliminates water uptake completely. In real coatings other parameters such as breathability must be maintained in a reasonable range necessitating a compromise in the extent to which the surface can be sealed. Figure 21 shows the %RC for each of the three coatings in this treatment group.

Figure 21: %RC for D, D/S and D/S/F treatments

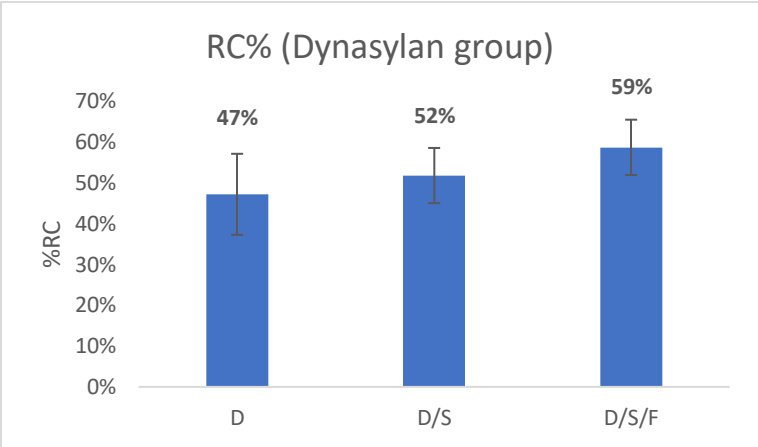

Treatment D shows a 47 ± 9.9 % reduction in water uptake compared to 52 ± 6.8% for the D/S and 59 ± 6.8% for the D/S/F treatment. In previous studies, a similar nanocomposite coating deposited on marble and consisting of siloxane, fluoropolymer, and silica nanoparticles was shown to reduce water penetration into stone by 75.1% [86] Another composite coating consisting of an amino/fluoro-modified polysiloxane and calcium hydroxide nanoparticles resulted in an RC% = 73% [99]. The D/S/F nanocomposite gave a result in the ballpark of what is expected for such a coating.

The Protectosil SC treatment group was also tested for reduction in water uptake through capillary action and figure 22 shows the amount of water absorbed by the specimen per unit area, Q_i (g/m^2) plotted against the square root of contact time with the capillary transport medium.

Figure 22: Plot of Q against $t^{1/2}$ for the Protectosil SC group

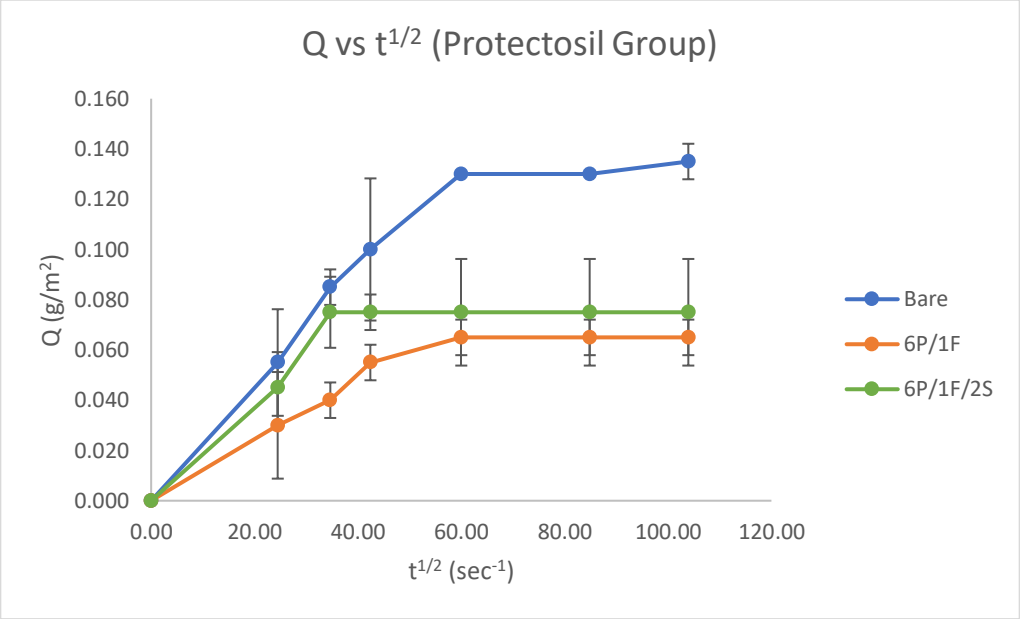

Intuitively, marble once again absorbs more water before surface treatments. The 6P/1F treatment reduces water uptake by capillarity by about 52% compared to bare marble. Figure 23 summaries the %RC results for this group.

Despite corresponding to a much higher initial SCA of 160.3° ± 2.5 compared to the 130.7 ° ± 1.2 of the 6P/1F coating, the nanocomposite 6P/1F/2S affords less protection from water penetration (RC = 44.4%) than the latter (RC = 52%). This is an unexpected result but as mentioned previously the water absorption by capillarity test is not the only parameter used to judge the performance of coatings. Having said that, it is possible that the superamphiphobic coating is fragile to prolonged contact with water which may cause cracking, thereby compromising the level of protection provided by the coating. The presence of fractures in siloxane-based products on stone materials has been reported in multiple studies [102], [144], [145] as products which polymerize through a sol-gel route [146,147] frequently exhibit cracks. These cracks are ascribed to shrinkage phenomena taking place throughout the drying phase [148]. Others tests carried out on this coating, potentially add weight to this theory. In future studies, SEM-imaging can help visualize these cracks if they exist. It has been shown that higher concentrations of siloxane-based hydrophobic coatings show more cracking [149] and that humid drying conditions can prevent cracking [150]. Therefore, perhaps by tweaking the proportions and modifying curing conditions a coating with better performance and durability can be fabricated.

Figure 23: %RC for 6P/1F and 6P/1F/2S treatments

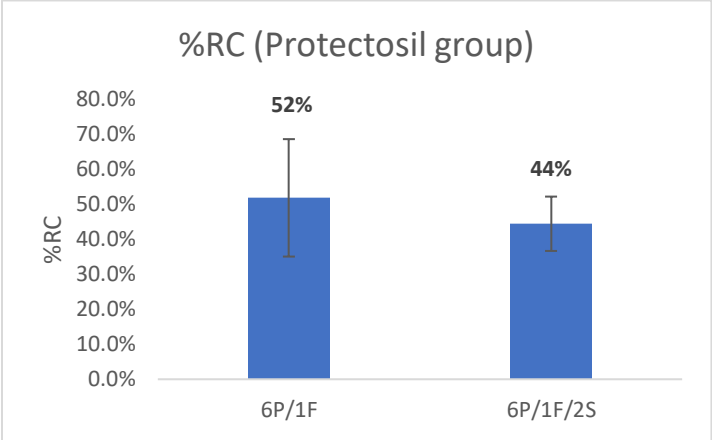

It may also be that the chemistry of the chosen polymer is not suited to create superhydrophobic composites through this route. In some cases, nanoparticle aggregates may cause drastic thinning of the protective coating in the inter-aggregate spaces. This could explain why the more hydrophobic coating offered less protection from water uptake. However, at this stage it is not clear if that is the case. Moreover, other parameters of wettability such as CAH and SA need to be measured to properly characterize the wettability of the surface treatments.

6.2 Water vapour permeability test

A coating that is designed for the protection of stone should not affect the water vapour transport properties of the stone [86]. An ideal but unrealistic scenario would be to observe no difference between the mass of vapour flow across treated and untreated samples corresponding to %RVP = 0%. Instead, a minimal possible reduction in permeability post treatment is aspired towards, as a drastic decrease in this parameter may activate the material's decay. If layers with different water vapour permeability are present in the stone, water may condensate inside the pores generating detrimental mechanical stress. This phenomenon may occur, particularly at the interface between

the untreated and treated parts with possible consequent detachments [88]. For this reason, the vapour permeability test was set up to quantify if and to what extent vapour diffusion and evapouration through the stone was negatively impacted post surface treatment.

Multiple experimental runs were set up and many months' worth of data collected while simultaneously optimizing the protocol. Only the fourth and fifth attempts achieved steady vapour flow according to the 2% criterion of (9). These included two bare marble samples (5^{th} attempt), two 6P/1F samples (4^{th} attempt) and one D/S/F sample (5^{th} attempt). The reduction in vapour permeability result for the D/S/F and 6P/1F treatments is summarized in figure 24.

Figure 24: %RVP for samples obeying the 2% criteria

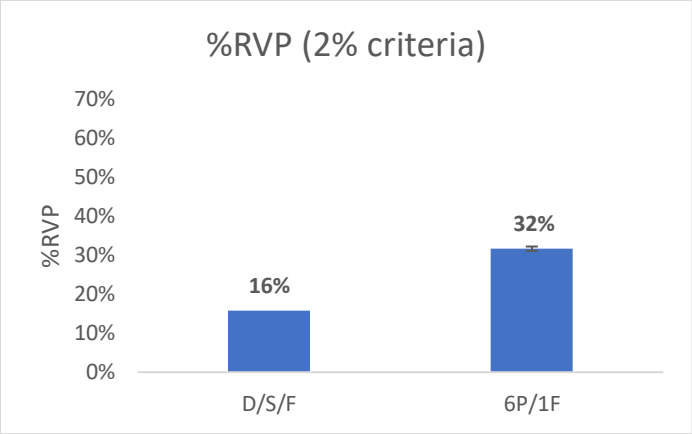

Silane and silicone-derived coatings are known to maintain a high degree of permeability to water vapour allowing stones to breathe [65]. The superhydrophobic D/S/F nanocomposite shows only 16% reduction in vapour permeability compared to bare marble which is a good result. The 6P/1F treatment shows a greater reduction of breathability by 32%. It has been reported that the average RVP% on white marble treated by a superhydrophobic composite material was 16.8% [86]. The

close correspondence of our result with expected values adds weight to the %RVP for the D/S/F coating.

Albeit the 6P/1F/2S superamphiphobic coating did not meet the 2% criterion for steady state vapour flow. Some useful information may be drawn by considering a laxer 5% cut off for steady vapour flow that has been used previously [143] and corresponds to (12),

$$\frac{\Delta M_i - \Delta M_{i-1}}{\Delta M_i} \times 100 < 5\% \qquad (12)$$

If we consider this new criterion (12) two additional 6P/1F treatments (5th attempt), in excellent agreement with the 6P/1F samples (4th attempt) meeting the 2% criterion, also achieve steady state. Additionally, three samples of 6P/1F/2S meet the 5% criterion as well and are in excellent agreement with each other across two separate experimental runs. Figure 25 summarizes the reduction in vapour permeability results following this 5% criteria for steady vapour flow.

Figure 25: %RVP for samples obeying the 5% criteria

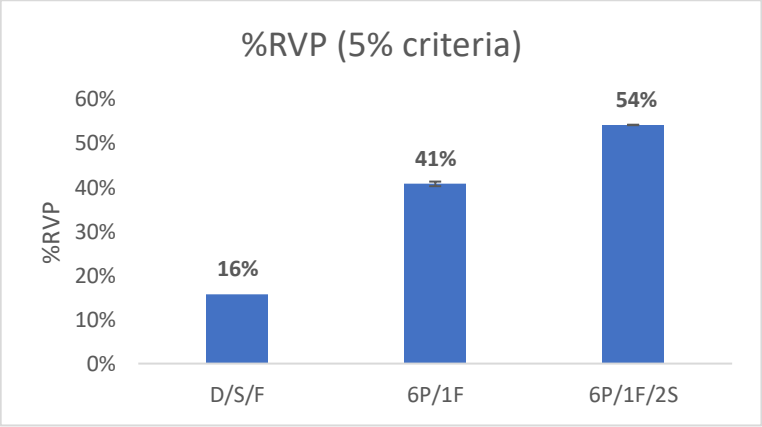

In figure 25 the 6P/1F/2S coating is associated with a reduction in stone breathability by 54%. The 6P/1F result is slightly modified by considering the additional two vapour loss values that bring down the central value to a lower more tightly clustered one. Therefore, the resulting reduction in breathability is slightly more pronounced.

The coatings overall seem to show reasonable breathability for the marble. However, more samples set up in the optimized protocol can validate these results further. The Protectosil treatment group shows repeatability in results increasing the confidence associated with results of this group. The D/S/F coating results are based on one sample alone but correspond perfectly to values reported in literature [86].

6.3 Sandpaper abrasion test

Mechanical durability is a major application-oriented concern for materials synthesized for use as water repellent coatings, particularly because a large volume of fabricated superhydrophobic surfaces abrade readily due to the delicate nature of their surface texture [136], [137]. Sometimes little more than brushing with a tissue is sufficient to destroy the fabricated surface. Moreover, many studies in heritage science neglect to test this vital parameter in the development of coatings for heritage applications. Therefore, multiple tests were employed in this work to evaluate the resilience of the synthesized coatings, the first being the sandpaper abrasion test. This test has not been applied to materials developed for use in cultural heritage before as it is considered a harsh measure of durability.

Three treatments belonging to the Dynasylan group i.e., D, D/S and D/S/F were tested using the sandpaper abrasion test. Figures 26, 27 and 28 show the WCA plotted against abrasion cycles for this treatment group.

Figure 26: WCA variation with abrasion cycles for D

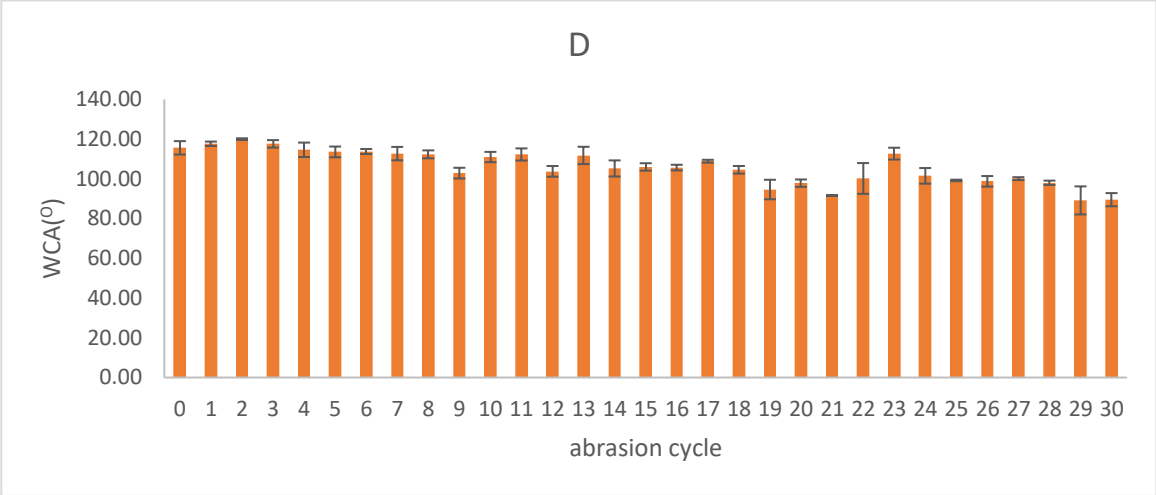

Figure 27: WCA variation with abrasion cycles for D/S

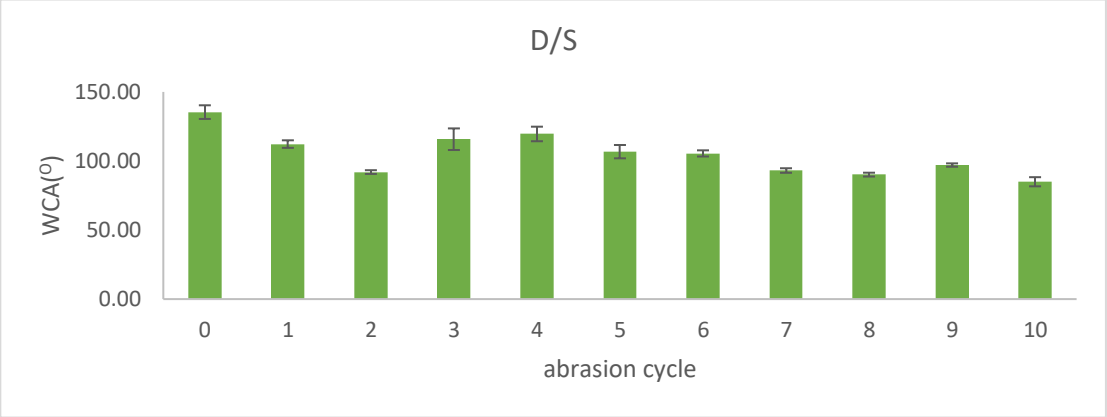

Figure 28: WCA variation with abrasion cycles for D/S/F

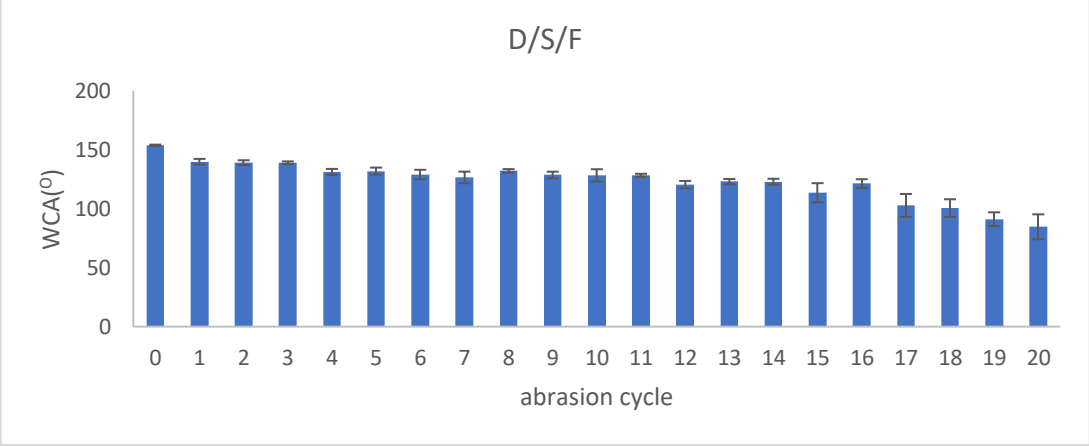

Treatment D maintained its hydrophobicity for approximately 30 cycles of abrasion. However, treatment D/S lost its enhanced hydrophobicity after just the first cycle of abrasion and lost hydrophobicity completely by the 9^{th} cycle. During the first cycle of abrasion white powders were found on the sandpaper. From other studies [131] it is well substantiated that these are floating/partially embedded nanoparticles. Since the interparticle forces between nanoparticles are weak these NPs are particularly vulnerable to abrasion. The addition of fluoropolymer in treatment D/S/F afforded physical support to the partially embedded nanoparticles consequently increasing the resilience of the coating. The D/S/F treatment showed a very promising result maintaining enhanced hydrophobicity up to 16 cycles of abrasion.

6.4 Tape peeling test

The sandpaper abrasion test was a harsh mechanism to test the mechanical durability of the synthesized coatings. A second, milder durability test was also set up. The same treatments i.e., D, D/S and D/S/F were tested and their WCA was plotted against tape peeling cycles in figures 29, 30 and 31 respectively.

Treatment D maintained its hydrophobicity even after 100+ cycles. Treatment D/S maintained enhanced hydrophobicity for 5 cycles (compared to the one in the case of sandpaper abrasion) and lost hydrophobicity completely after 16 cycles. The D/S/F treatment maintained enhanced hydrophobicity for up to 25 cycles and remained weakly hydrophobic for 50+ cycles.

Figure 29: WCA variation with tape peeling cycles for D

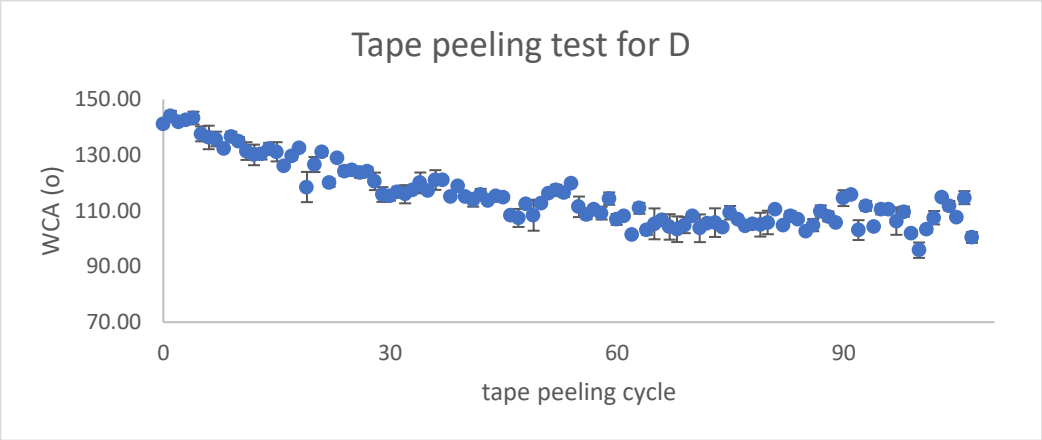

Figure 30: WCA variation with tape peeling cycles for D/S

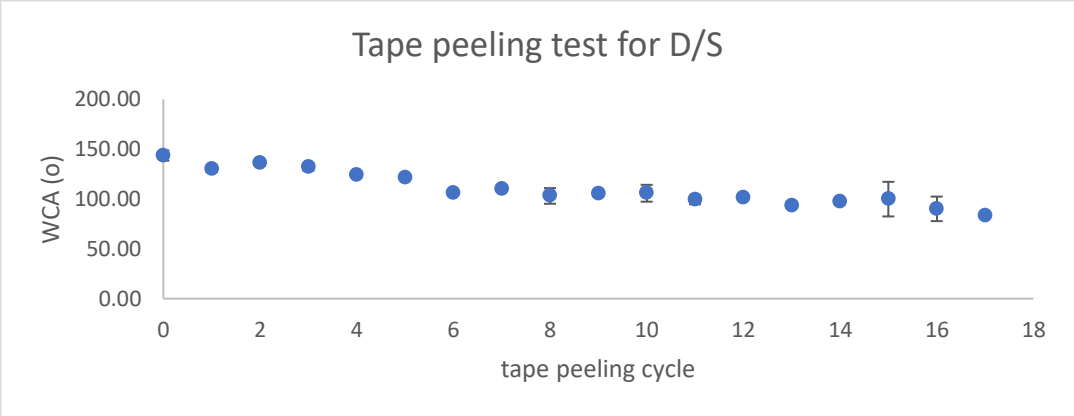

Figure 31: WCA variation with tape peeling cycles for D/S/F

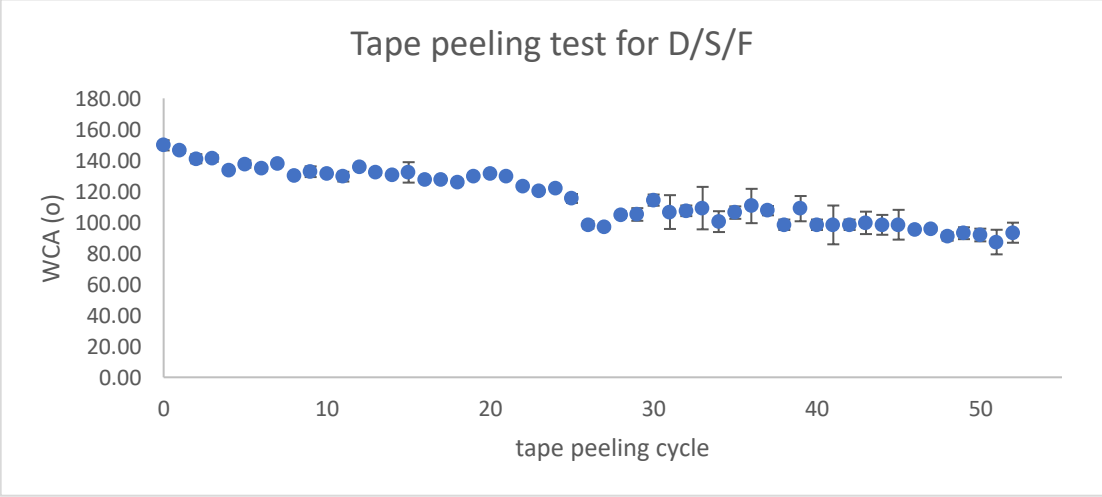

Intuitively, the tape peeling test reproduced the same trend as the sandpaper abrasion test. D showed the most resilience to abrasion, as is expected from a pure polymer system, and the D/S treatment was once again found to be quite fragile to abrasion. This demonstrates the need for fluoropolymer use to stabilize the SiO_2 nanoparticles in the polymer matrix. The superhydrophobic D/S/F treatment tolerated 50+ peeling cycles indicating very good mechanical durability.

6.5 Freeze-thaw test

Ice/frost accretion in moist conditions is a typical thorny case to weaken the superhydrophobicity and shorten the service life of water repellent products. Therefore, the coatings were tested in their ability to tolerate cycles of freezing and thawing that measures their mechanical robustness in extreme temperatures [133].

This test was carried out on the Protectosil treatment group whose mechanical durability was not tested by the sandpaper abrasion and tape peeling tests. Both the 6P/1F and 6P/1F/2S treatments maintained their enhanced hydrophobicity over twenty cycles of freezing and thawing. The results can be visualized in figures 32 and 33.

Figure 32: WCA against freeze-thaw cycle for two samples of 6P/1F

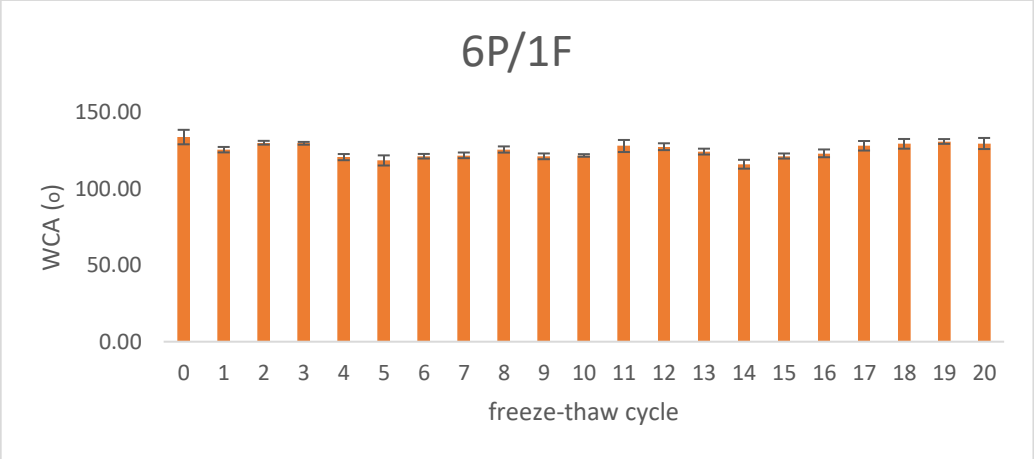

Figure 33: WCA against freeze-thaw cycle 6P/1F/2S

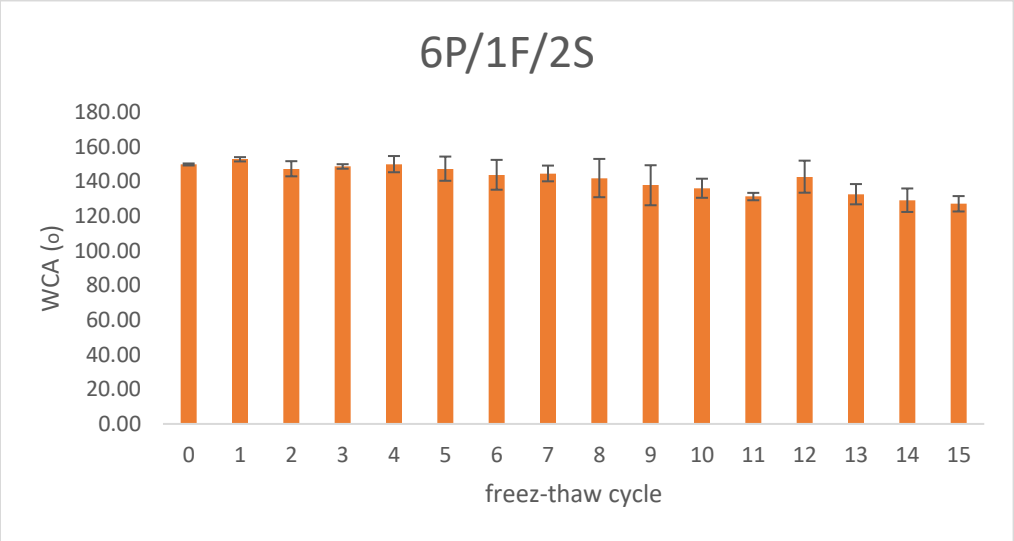

6.6 Acid/ rain simulation test

The rain simulation test was also performed on the Protectosil treatment group. The results for the 6P/1F and 6P/1F/2S treatments can be visualized in figure 34.

Figure 34: Rain test for the Protectosil group

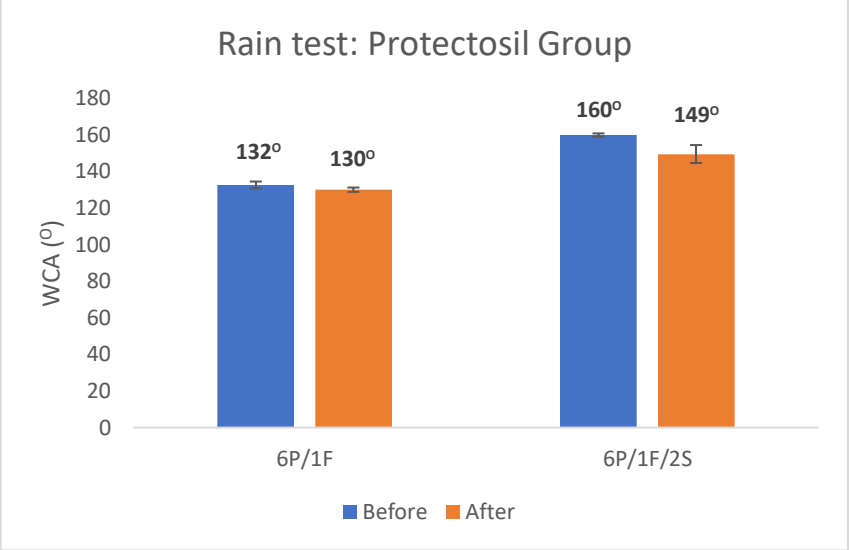

The 6P/1F coating was durable in the face of simulated rainfall with its WCA dropping only slightly from 132 ±1.89° to 130 ±1.19°. The 6P/1F/2S treatment also gave a good result with its WCA transforming from 160 ± 0.88° to 149 ±4.91°. It is worth mentioning that the result for the 6P/1F coating showed repeatability but that of the 6P/1F/2S coating did not. Further testing under acid rain, however, confirmed that the 6P/1F/2S coating did retain stability across acid/rain cycles. This raised a potential issue with the experimental set up/protocol that needs optimization to eliminate the inaccuracy in some repeat samples of 6P/1F/2S.

The use of distilled water during the rain test means that it is a measure of durability in response to water impact. To simulate rain in urban environments more realistically, another version of the test was performed with acidified water (pH ~4.3). The results for the Dynasylan and Protectosil groups are summarized in figures 35.

One sample of the D/S and both samples of the D/S/F treatment retained enhanced hydrophobicity upon exposure to artificial acid rain. The 6P/1F treatment gave the same result across the water impact and acid rain tests. Other studies have shown superhydrophobic polysiloxane-SiO_2 NP coatings offering good resilience to immersion in strong acid/base solutions [142]. Consequently, their high tolerance to acidified rain is substantiated.

Figure 35: Acid rain test for both groups

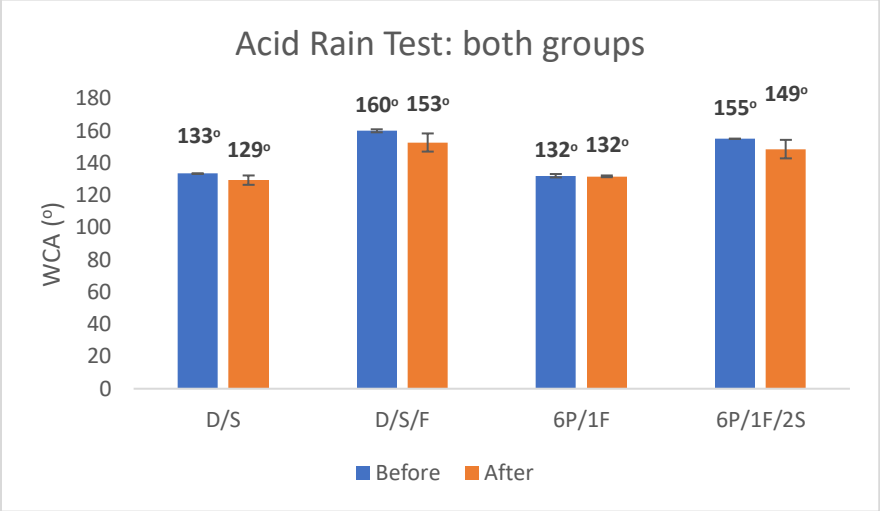

6.7 Sand-grit erosion test

Yet another test for durability, the sand-grit erosion test was performed on both treatment groups. The D/S treatment lost hydrophobicity after 10 cycles of sand-grit erosion (figure 36). Interestingly the D/S/F coating also took the same number of cycles to be destroyed (figure 37).

Figure 36: WCA against sand-grit erosion cycle for D/S

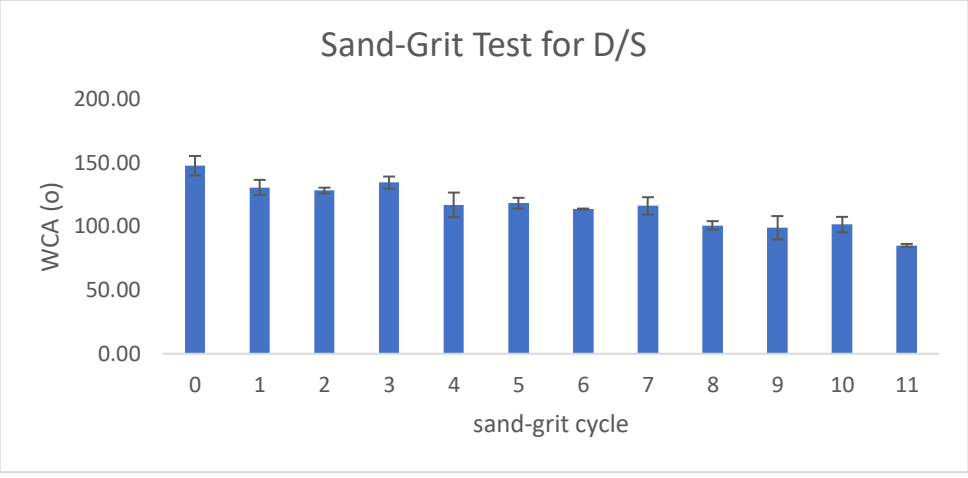

Figure 37: WCA against sand-grit erosion cycle for D/S/F

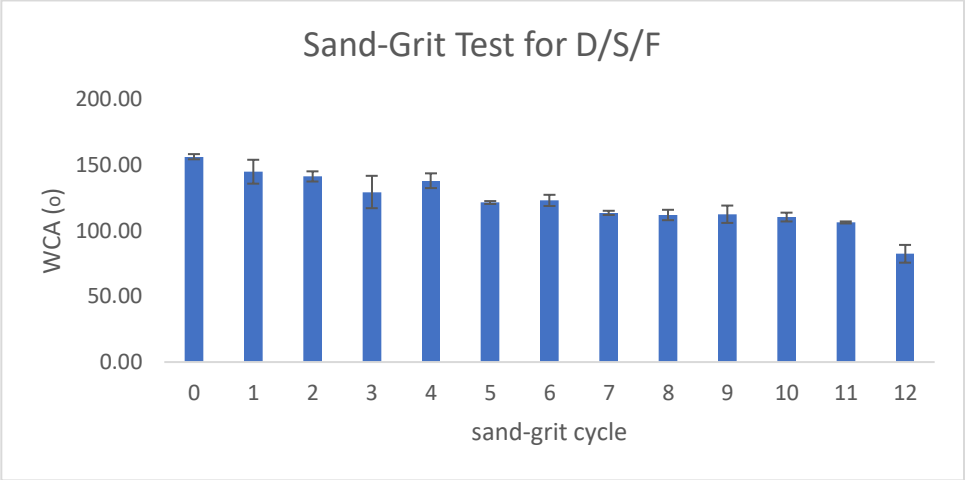

In the Protectosil group, the 6P/1F showed great results affirming its good mechanical robustness demonstrated in other tests as well. Hydrophobicity was maintained for 46 cycles of sand-grit erosion (figure 38). The 6P/1F/2S was, however, found to possess poor durability as it lost hydrophobicity in one cycle of sand-grit erosion going from a WCA of 159.9^{o} to that of 84^{o}.

Figure 38: WCA against sand-grit erosion cycle for 6P/1F

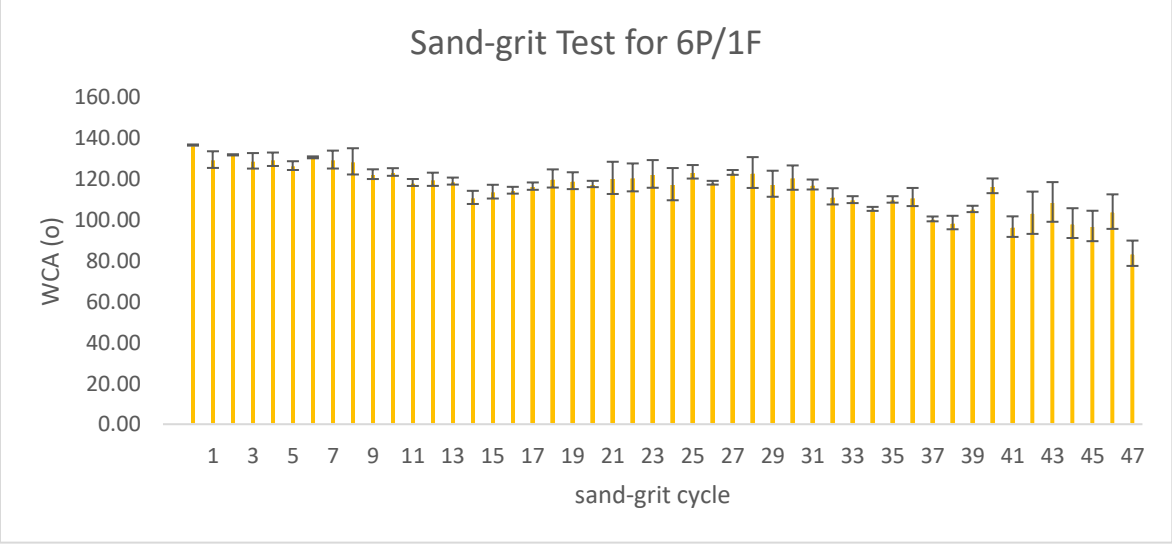

6.8 Accelerated UV-aging test

An accelerated aging experiment using UV irradiation was used to investigate the anti-aging performance of the four treatments viz. D/S, D/S/F, 6P/1F and 6P/1F/2S. All treatments retain enhanced hydrophobicity after ~2 months (1344 hours) of accelerated aging in the UVA chamber.

Figure 39: UV-Aging for the Dynasylan group

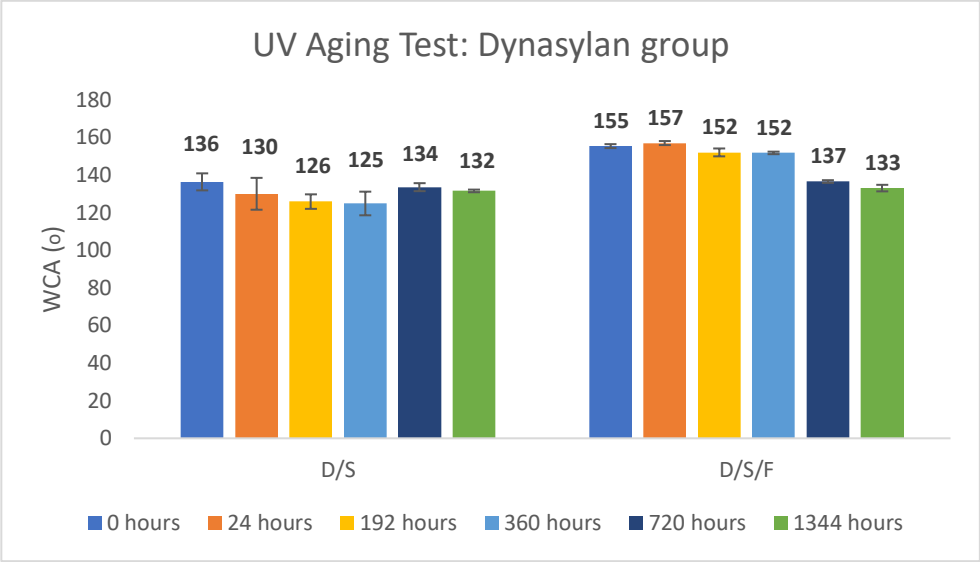

Figure 40: UV-Aging for the Protectosil group

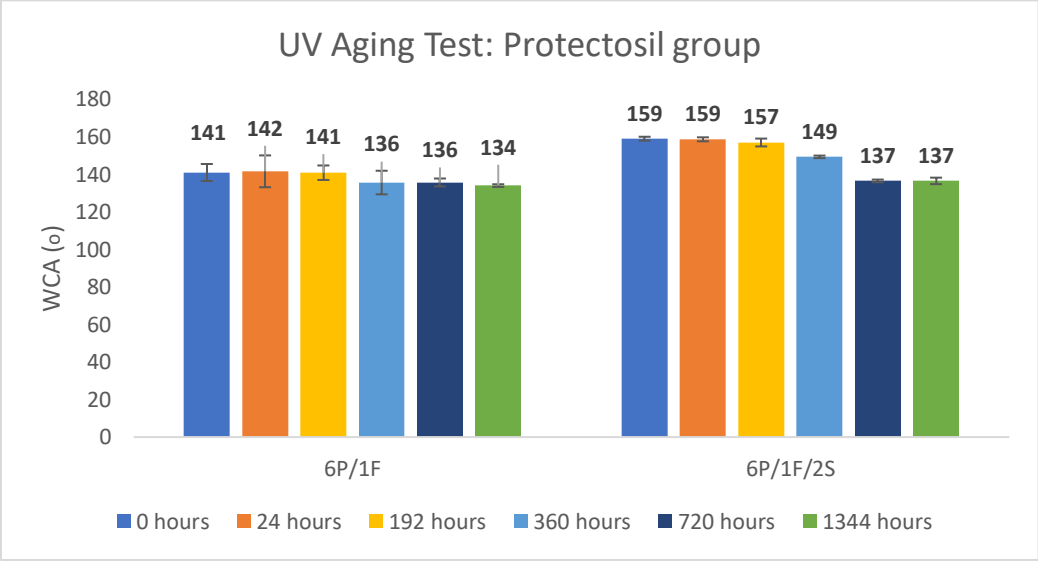

Previous studies have drawn positive correlations between the presence of fluoropolymer and nanoscale roughness and the coating's resistance to UV degradation. The close stacked nano-SiO_2 particles have been hypothesized to form a dense surface structure with a uniform nano-roughness which can act as a protective layer for the coating enabling UV resistance [140]. However, the irradiation intensity in our experiments was kept at a low 1.064 W/m^2 similar to Huang et al. [154]. Others have also used higher intensities in the 60-180 W/m^2 range as well [140]. In the future, the coatings should be tested at greater irradiation intensity and for longer periods of exposure. Other studies have also utilized higher temperatures in the climatic chamber accompanied by regular cooling incorporated into the protocol. Moreover, gloss assessments can give us interesting data to work with as well [140].

Our data suggests that all treatments show good results by maintaining enhanced hydrophobicity through two months of UV exposure. No conclusion can be drawn about the effect of fluoropolymer and nanoscale roughness on rate of accelerated aging at this stage.

7 Conclusion

Nature is abundant in surfaces that display special non-wetting behaviours caused by a multiscale hierarchal roughness combined with materials that lower surface energy. Prior to this work, a biomimetic route was used to fabricate a superhydrophobic coating, D/S/F (WCA=160°) and another superamphiphobic coating, 6P/1F/2S (WCA=160.3°, OCA=152.2°) on marble. Both coatings did not affect the original colour of the marble substrate ($\Delta E^* < 5.0$). This research project assessed the performance of these novel coatings by characterizing their water uptake behaviour through the water absorption by capillarity test, breathability through the vapour permeability test, mechanical durability through the sandpaper abrasion and tape peeling tests, response to environmental degradation agents through the freeze-thaw, acid/rain simulation and sand-grit erosion tests, and finally, their response to accelerated UV-aging. Furthermore, it also helped develop and optimize the test protocols used to assess novel coatings designed for stone protection. A great emphasis was placed on mechanical durability assessment which is an often neglected in the development of materials destined for application in the field of heritage. The D/S/F coating offered better protection against water absorption by capillary (%RC = 59 ± 6.8%) compared to the pure hydrophobic binder (%RC = 47 ± 9.9%) i.e., a 25% improvement in protection compared to the commercial product. The coating achieved this while reducing the stone's breathability by only ~16% and showing good mechanical durability evidenced by the maintenance of enhanced hydrophobicity through 16 cycles of the sandpaper abrasion test, which, to the best of our knowledge, has not been applied to heritage studies prior to this work. The coating also maintained hydrophobicity for 50+ tape peeling cycles and was also resilient to acid/rain simulation and sand-grit erosion. Overall, the coating showed an improvement in protection against water penetration with minimal to negligible associated negative impacts and promising durability. The 6P/1F/2S

coating, however, did not show improved protection from water uptake through capillarity, which is not a reliable criterion on its own to judge the performance of a coating. The treatment also resulted in a ~54% reduction of breathability in the stone and was found to be vulnerable to the very harsh sand-grit erosion test but tolerant to at least 15 freeze-thaw cycles and acid/rain simulation. Moreover, both the coating maintained their enhanced hydrophobicity over two months of accelerated UV-aging. This coating offers potential that can be explored further by running other tests and investigating if any modifications can improve the associated breathability. Since this coating is superamphiphobic, its anti-graffiti protection can also be explored in the future. This body of work helped unveil the performance and durability of two novel coatings displaying extreme wetting behaviours by using a methodology that is heritage-application oriented.

References

[1] UNESCO World Heritage Centre, “What is world heritage?,” *UNESCO World Heritage Centre*. [Online]. Available: https://whc.unesco.org/en/faq/19. [Accessed: 12-Nov-2022].

[2] S. Kanani and H. Zandi, “A Study of the Damages to Historical Monuments due to Climatic Factors and Air Pollution and offering solutions,” *International Journal of Humanities and Social Sciences*, vol. 5, no. 8, pp. 1018–1021, 2011.

[3] C. Alves, C. A. Figueiredo, J. Sanjurjo-Sánchez, and A. C. Hernández, “Effects of water on natural stone in the built environment-a review,” *Geosciences*, vol. 11, no. 11, 2021.

[4] L. de Ferria Pier Paolo Lottici Andrea Lorenzi Angelo Montenero Emma Salvioli-Mariani, “Study of silica nanoparticles – polysiloxane hydrophobic treatments for stone-based monument protection,” *Journal of Cultural Heritage*, vol. 12, no. 4, pp. 356–363.

[5] C. N. W. Barthlott, “Purity of the sacred lotus, or escape from contamination in biological surfaces,” *Planta*, vol. 202, no. 1, pp. 1–8.

[6] Taolei Sun, Lin Feng, Xuefeng Gao, and Lei Jiang, “Bioinspired Surfaces with Special Wettability,” *Acc. Chem. Res*, vol. 38, no. 8, pp. 644–652, May 2005.

[7] S. H. Alexander Otten, “How Plants Keep Dry: A Physicist’s Point of View,” *Langmuir*, vol. 20, no. 6, pp. 2405–2408, Feb. 2004.

[8] P. Wagner, R. Fu rstner, W. Barthlott, C. Neinhuis, “Quantitative assessment to the structural basis of water repellency in natural and technical surfaces,” *Journal of Experimental Botany*, vol. 54, no. 385, pp. 1295–1303, Apr. 2003.

[9] L. Feng *et al.*, “Super-hydrophobic surfaces: From natural to artificial,” *Adv. Mater.*, vol. 14, no. 24, pp. 1857–1860, 2002.

[10] L. J. Xuefeng Gao, “Water-repellent legs of water striders,” *Nature*, vol. 432, p. 36, Nov. 2004.

[11] T. Wagner, C. Neinhuis, and W. Barthlott, “Wettability and contaminability of insect wings as a function of their surface sculptures,” *Acta Zool.*, vol. 77, no. 3, pp. 213–225, 1996.

[12] M. Svoboda, A. Malijevský, and M. Lísal, “Wetting properties of molecularly rough surfaces,” *J. Chem. Phys.*, vol. 143, no. 10, p. 104701, 2015.

[13] Y.-Z. Hu and T.-B. Ma, “Tribology of Nanostructured Surfaces,” in *Comprehensive Nanoscience and Technology*, Elsevier, 2011, pp. 383–418.

[14] “Contact angle,” *Biolinscientific.com*. [Online]. Available: https://www.biolinscientific.com/measurements/contact-angle. [Accessed: 12-Nov-2022].

[15] Y. Jiang and C.-H. Choi, “Droplet retention on superhydrophobic surfaces: A critical review,” *Adv. Mater. Interfaces*, vol. 8, no. 2, p. 2001205, 2021.

[16] T. Young, “An essay on the cohesion of fluids,” *Philos Trans R Soc Lond*, vol. 95, pp. 65–87, 1805.

[17] E. A. Vogler, “Structure and reactivity of water at biomaterial surfaces,” *Adv Colloid Interface*, vol. 74, pp. 69–117, 1998.

[18] C. Guo, S. Wang, H. Liu, L. Feng, Y. Song, and L. Jiang, “Wettability alteration of polymer surfaces produced by scraping,” *J Adhes Sci Technol*, vol. 22, pp. 395–402, 2008.

[19] Ioannis Karapanagiotis, Ioannis Poulios, Aikaterini Chatzigrigoriou, Tobin Kopp, “Superhydrophobic and Self-Cleaning Coatings for the Protection of the Cultural Heritage: A Case Study Using TiO2 Nanoparticles,” in *Materials with extreme wetting properties: Methods and emerging industrial applications*, 1st ed., M. Hosseini and I. Karapanagiotis, Eds. Cham, Switzerland: Springer International Publishing, 2021, pp. 209–232.

[20] M. H. Ioannis Karapanagiotis, “Superhydrophobic Coatings for the Protection of Natural Stone,” in *Advanced materials for the conservation of stone*, M. Hosseini and I. Karapanagiotis, Eds. Cham, Switzerland: Springer International Publishing, 2019, pp. 1–25.

[21] Jiaqiang *et al.*, “Wetting models and working mechanisms of typical surfaces existing in nature and their application on superhydrophobic surfaces: A review,” *Adv. Mater. Interfaces*, vol. 5, no. 1, p. 1701052, 2018.

[22] R. N. Wenzel, “RESISTANCE OF SOLID SURFACES TO WETTING BY WATER,” *Ind. Eng. Chem*, vol. 28, p. 988, Aug. 1936.

[23] S. B. A. B. D. Cassie, “Wettability of porous surfaces,” *Trans. Faraday Soc*, vol. 40, pp. 541–551, 1944.

[24] P. N. Manoudis, I. Karapanagiotis, A. Tsakalof, I. Zuburtikudis, and C. Panayiotou, “Superhydrophobic composite films produced on various substrates,” *Langmuir*, vol. 24, no. 19, pp. 11225–11232, 2008.

[25] “Petal effect: a superhydrophobic state with high adhesive force,” *Langmuir*, vol. 24, no. 8, pp. 4114–4119, 2008.

[26] W. Chen, A. Y. Fadeev, M. C. Hsieh, D. Öner, J. Youngblood, and T. J. McCarthy, "Ultrahydrophobic and ultralyophobic surfaces: Some comments and examples," *Langmuir*, vol. 15, no. 10, pp. 3395–3399, 1999.

[27] T. J. M. Didem Öner, "Ultrahydrophobic Surfaces. Effects of Topography Length Scales on Wettability," *Langmuir*, vol. 16, no. 20, pp. 7777–7782, Aug. 2000.

[28] E. Wolfram, R. I. Faust, and J. F. Wetting ; Padday, *Spreading and Adhesion*. London: Academic Press, 1978.

[29] Wei Chen, Alexander Y. Fadeev, Meng Che Hsieh, Didem Öner, Jeffrey Youngblood, and Thomas J. McCarthy, "Ultrahydrophobic and ultralyophobic surfaces: some comments and examples," *langmuir*, vol. 15, no. 10, pp. 3395–3399.

[30] R. J. Good, "A Thermodynamic Derivation of Wenzel's Modification of Young's Equation for Contact Angles; Together with a Theory of Hysteresis," *J Am Chem Soc.*, vol. 74, no. 20, pp. 5041–5042, Oct. 1952.

[31] R. H. D. Rulon E. Johnson Jr, "Contact Angle Hysteresis. III. Study of an Idealized Heterogeneous Surface," *J. Phys. Chem.*, vol. 68, no. 7, pp. 1744–1750, Jul. 1964.

[32] D. Staley, "Biomimicry: A history," *Osu.edu*. [Online]. Available: https://ehistory.osu.edu/exhibitions/biomimicry-a-history. [Accessed: 12-Nov-2022].

[33] Y. Bar-Cohen, *Biomimetics Nature-Based Innovation*. Bosa Roca: CRC Press, 2012.

[34] K. Koch, B. Bhushan, and W. Barthlott, "Multifunctional Surface Structures of Plants: An Inspiration for Biomimetics," *Biomimetics. Prog. Mater. Sci*, vol. 54, pp. 137–178, 2009.

[35] Yan-Ling Wan, Jun Lou, Zhan-Jiang Yu, Xiao-Zhou Li, Hua-Dong Yu, "Single-step fabrication of bionic-superhydrophobic surface using reciprocating-type high-speed wire cut electrical discharge machining," *Chinese Science Bulletin*, vol. 59, p. 3691, Jul. 2014.

[36] W. L. Zhiguang Guo, "Biomimic from the superhydrophobic plant leaves in nature: Binary structure and unitary structure," *Plant Science*, vol. 172, no. 6, p. 1103, Jun. 2007.

[37] "History of electron microscopy, 1931-2000," *Caltech.edu*. [Online]. Available: https://authors.library.caltech.edu/5456/1/hrst.mit.edu/hrs/materials/public/ElectronMicroscope/EM_HistOverview.htm. [Accessed: 12-Nov-2022].

[38] W. B. C. Neinhuis, "Characterization and Distribution of Water-repellent, Self-cleaning Plant Surfaces," *Ann. Bot.*, vol. 79, no. 6, p. 667, Jun. 1997.

[39] A. N. K. H. Watanabe, "Recent Studies on Super-Hydrophobic Films," *Monatshefte für Chemie*, vol. 132, p. 31, Jan. 2001.

[40] L. Feng, S. Li, Y. Li, H. Li, L. Zhang, J. Zhai, Y. Song, B. Liu, L. Jiang, D. Zhu, "Super-Hydrophobic Surfaces: From Natural to Artificial," *Advanced Materials*, vol. 14, no. 24, pp. 1857–1860, 2002.

[41] M. Ghasemlou, F. Daver, E. P. Ivanova, and B. Adhikari, "Bio- Inspired Sustainable and Durable Superhydrophobic Materials: From Nature to Market," *J. Mater. Chem*.

[42] K. Manoharan and S. Bhattacharya, "Superhydrophobic surfaces review: Functional application, fabrication techniques and limitations," *J. micromanufacturing*, vol. 2, no. 1, pp. 59–78, 2019.

[43] A D Tserepi, M-E Vlachopoulou, E Gogolides, "Nanotexturing of poly(dimethylsiloxane) in plasmas for creating robust super-hydrophobic surfaces," *Nanotechnology*, vol. 17, pp. 3977–3983, 2006.

[44] Hiroshi Yabu, Masafumi Takebayashi, Masaru Tanaka, Masatsugu Shimomura, "Superhydrophobic and lipophobic properties of self-organized honeycomb and pincushion structures," *Langmuir*, vol. 21, pp. 3235–3237, 2005.

[45] J.-D. H. Gero Decher, "Buildup of ultrathin multilayer films by a self-assembly process, 1 consecutive adsorption of anionic and cationic bipolar amphiphiles on charged surfaces," *Makromolekulare Chemie. Macromolecular Symposia*, vol. 46, p. 321, 1991.

[46] N. Zhao, F. Shi, Z. Wang, and X. Zhang, "Combining layer-by-layer assembly with electrodeposition of silver aggregates for fabricating superhydrophobic surfaces," *Langmuir*, vol. 21, no. 10, pp. 4713–4716, 2005.

[47] Lei Zhai, Fevzi Ç. Cebeci, Robert E. Cohen, and Michael F. Rubner, "Stable Superhydrophobic Coatings from Polyelectrolyte Multilayers," *Nano Letters*, vol. 4, p. 1349, 2004.

[48] Jiadao Wang, Ang Li, Haosheng Chen, Darong Chen, "Synthesis of biomimetic superhydrophobic surface through electrochemical deposition on porous alumina," *Journal of Bionic Engineering*, vol. 8, pp. 122–128, 2011.

[49] G. S. Yin Li, "Electrochemical Growth of Two-Dimensional Gold Nanostructures on a Thin Polypyrrole Film Modified ITO Electrode," *J. Phys. Chem. B*, vol. 109, no. 50, pp. 23787–23793, 2005.

[50] F. Shi, Y. Song, J. Niu, X. Xia, Z. Wang, and X. Zhang, "Facile method to fabricate a large-scale superhydrophobic surface by galvanic cell reaction," *Chem. Mater.*, vol. 18, no. 5, pp. 1365–1368, 2006.

[51] S.Shibuichi, T. Yamamoto, T. Onda, K. Tsujii, "Super Water- and Oil-Repellent Surfaces Resulting from Fractal Structure," *Journal of Colloid and Interface Science*, vol. 208, no. 1, pp. 287–294, 1998.

[52] N. J. Shirtcliffe, G. McHale, M. I. Newton, C. C. Perry, “Intrinsically superhydrophobic organosilica sol-gel foams,” *Langmui*, vol. 19, pp. 5626–5631, 2003.

[53] Masaya Hikita, Keiji Tanaka, Tetsuya Nakamura, Tisato Kajiyama, Atsushi Takahara, “Super-liquid-repellent surfaces prepared by colloidal silica nanoparticles covered with fluoroalkyl groups,” *langmui*, vol. 21, pp. 7299–7302, 2005.

[54] H. B. B. Mahltig, “Modified Silica Sol Coatings for Water-Repellent Textiles,” *Journal of Sol-Gel Science and Technology*, vol. 27, pp. 43–52, 2003.

[55] A. V. A. R. J. R. Pedro J. Rivero, *Electrospinning Technique as a Powerful Tool for the Design of Superhydrophobic Surfaces*. 2020.

[56] Minglin Ma, Randal M Hill, Joseph L Lowery, Sergey V Fridrikh, Gregory C Rutledge, “Electrospun poly(styrene-block-dimethylsiloxane) block copolymer fibers exhibiting superhydrophobicity,” *langmuir*, vol. 21, pp. 5549–5554, 2005.

[57] Yushan Yang, Haishan He, Yougui Li, Jian Qiu, “Using Nanoimprint Lithography to Create Robust, Buoyant, Superhydrophobic PVB/SiO2 Coatings on wood Surfaces Inspired by Red roses petal,” *Scientific Reports*, vol. 9, p. 9961, 2019.

[58] B. Qian and Z. Shen, “Fabrication of superhydrophobic surfaces by dislocation-selective chemical etching on aluminum, copper, and zinc substrates,” *Langmuir*, vol. 21, no. 20, pp. 9007–9009, 2005.

[59] Juan Lv, Zhengjun Gong, Zhoukun He, Jian Yang, Yanqiu Chen, Changyu Tang, Yu Liu, Meikun Fan, Woon-Ming Lauc, “3D printing of a mechanically durable superhydrophobic porous membrane for oil–water separation,” *Journal of materials chemistry A*, vol. 5, pp. 12435–12444, May 2017.

[60] K. Lee, H. Park, and D. Chun, *Fabrication of superhydrophobic surface by 3D printing and dip coating*. .

[61] Yang Yang, Xiangjia Li, Xuan Zheng, Zeyu Chen, Qifa Zhou, Yong Chen, “3D-Printed Biomimetic Super-Hydrophobic Structure for Microdroplet Manipulation and Oil/Water Separation,” *Advanced Materials*, vol. 30, no. 9, p. 1704912, Dec. 2017.

[62] I. Karapanagiotis and P. N. Manoudis, “Superhydrophobic and superamphiphobic materials for the conservation of natural stone: An overview,” *Constr. Build. Mater.*, vol. 320, no. 126175, p. 126175, 2022.

[63] A. E. Charola, *Water-repellent treatments for building stones: A practical overview. APT Bull*, vol. 26. Los Angeles, CA, USA, 1995.

[64] G. Wheeler, “Alkoxysilanes and the Consolidation of Stone; The Getty Conservation Institute,” *Chapter*, vol. 1, pp. 1–11, 2005.

[65] P. Fermo *et al.*, “Hydrophobizing coatings for cultural heritage. A detailed study of resin/stone surface interaction,” *Appl. Phys. A Mater. Sci. Process.*, vol. 116, no. 1, pp. 341–348, 2014.

[66] Lucia Toniolo, Tommaso Poli, Valter Castelvetro, Antonella Manariti, Oscar Chiantore, Massimo Lazzari, “Tailoring new fluorinated acrylic copolymers as protective coatings for marble,” *Journal of cultural heritage*, vol. 3, p. 309, 2002.

[67] Linda Y. L. Wu, G. H. Tan, X. T. Zeng, T. H. Li, Z. Chen, “Synthesis and Characterization of Transparent Hydrophobic Sol-Gel Hard Coatings,” *Journal of Sol-Gel Science and Technology*, vol. 198, p. 420, Apr. 2006.

[68] M. L. O. Chiantore, “Photo-oxidative stability of paraloid acrylic protective polymers,” *Polymer*, vol. 42, no. 1, pp. 17–27, Jan. 2001.

[69] C. A. P. Eric Doehne, *Stone Conservation: An Overview of Current Research (Second Edition)*. Santa Monica, CA: Getty Conservation Institute, 2010.

[70] M. M. Mariateresa Lettieri, “Performances and Coating Morphology of a Siloxane-Based Hydrophobic Product Applied in Different Concentrations on a Highly Porous Stone,” *Coatings*, vol. 6, no. 4, p. 60, 2016.

[71] G. Wheeler, *Alkoxysilanes and the consolidation of stone*. Los Angeles, CA: Getty Publications, 2005.

[72] P. Manoudis, S. Papadopoulou, I. Karapanagiotis, A. Tsakalof, I. Zuburtikudis, and C. Panayiotou, “Polymer-Silica nanoparticles composite films as protective coatings for stone-based monuments,” *J. Phys. Conf. Ser.*, vol. 61, pp. 1361–1365, 2007.

[73] M. Morra, E. Occhiello, and F. Garbassi, “Contact angle hysteresis in oxygen plasma treated poly(tetrafluoroethylene),” *Langmuir*, vol. 5, pp. 872–876, 1989.

[74] ´ D. Q.´re, “Rough ideas on wetting,” *Physica A*, vol. 313, pp. 32–46, 2002.

[75] R. H. D. Rulon E. Johnson, “Contact Angle Hysteresis I. Study of an Idealized Rough Surface,” *Advances in Chemistry*, vol. 43, pp. 112–135, 1964.

[76] Panagiotis N Manoudis, Ioannis Karapanagiotis, Andreas Tsakalof, Ioannis Zuburtikudis, Costas Panayiotou, “Superhydrophobic composite films produced on various substrates,” *Langmuir*, vol. 24, no. 19, pp. 11225–11232, Oct. 2008.

[77] P. N. Manoudis, A. Tsakalof, I. Karapanagiotis, I. Zuburtikudis, C. Panayiotou, “Fabrication of super-hydrophobic surfaces for enhanced stone protection,” *Surface and Coatings Technology*, vol. 203, no. 10–11, pp. 1322–1328, Feb. 2009.

[78] P. N. Manoudis and I. Karapanagiotis, “Modification of the wettability of polymer surfaces using nanoparticles,” *Prog Org Coat*, vol. 77, no. 2, pp. 331–338, 2014.

[79] L. de Ferri Pier Paolo Lottici Andrea Lorenzi Angelo Montenero Emma Salvioli-Mariani, “Study of silica nanoparticles–polysiloxane hydrophobic treatments for stone- based monument protection,” *journal of cultural heritage*, vol. 12, no. 4, pp. 356–363, 2011.

[80] P. M. F. M. Carcangiu, “Marble protection: An inorganic electrokinetic approach,” *Appl. Surf. Sci.*, vol. 273, pp. 377–385, May 2013.

[81] D. S. Facio and M. J. Mosquera, “Simple strategy for producing superhydrophobic nanocomposite coatings in situ on a building substrate,” *ACS Appl. Mater. Interfaces*, vol. 5, no. 15, pp. 7517–7526, 2013.

[82] A. Chatzigrigoriou, P. N. Manoudis, and I. Karapanagiotis, “Fabrication of water repellent coat- ings using waterborne resins for the protection of the cultural heritage,” *Macromol Symp*, no. 1, pp. 158–165, 2013.

[83] C. Esposito Corcione, R. Striani, and M. Frigione, “Hydrophobic photopolymerizable nanostructured hybrid materials: An effective solution for the protection of porous stones,” *Polym. Compos.*, vol. 36, no. 6, pp. 1039–1047, 2015.

[84] D. Aslanidou, I. Karapanagiotis, and C. Panayiotou, “Tuning the wetting properties of siloxane- nanoparticle coatings to induce superhydrophobicity and superoleophobicity for stone protec- tion,” *Mater Des*, vol. 108, pp. 736–744, 2016.

[85] D. Aslanidou, I. Karapanagiotis, and C. Panayiotou, “Superhydrophobic, superoleophobic coatings for the protection of silk textiles,” *Prog. Org. Coat.*, vol. 97, pp. 44–52, 2016.

[86] D. Aslanidou, I. Karapanagiotis, and D. Lampakis, “Waterborne superhydrophobic and superoleophobic coatings for the protection of marble and sandstone,” *Materials (Basel)*, vol. 11, no. 4, 2018.

[87] M. Lettieri, M. Masieri, A. Morelli, M. Pipoli, and M. Frigione, “Oleo/hydrophobic coatings containing nano-particles for the protection of stone materials having different porosity,” *Coatings*, vol. 8, no. 12, p. 429, 2018.

[88] M. Lettieri, M. Masieri, and M. Frigione, “Novel nano-filled coatings for the protection of built heritage stone surfaces,” *Nanomaterials (Basel)*, vol. 11, no. 2, p. 301, 2021.

[89] A. Fujishima, “TiO2 photocatalysis and related surface phenomena, Surf,” *Surf. Sci. Rep*, vol. 63, pp. 515–582, 2008.

[90] X. Chen and S. S. Mao, “Titanium dioxide nanomaterials: synthesis, properties, modifications, and applications,” *Chem. Rev.*, vol. 107, no. 7, pp. 2891–2959, 2007.

[91] J. Zhao and X. Yang, “Photocatalytic oxidation for indoor air purification: a literature review,” *Build. Environ.*, vol. 38, no. 5, pp. 645–654, 2003.

[92] C. A. Price, G. G. Amoroso, and V. Fassina, “Stone decay and conservation: Atmospheric pollution, cleaning, consolidation and protection,” *Stud. Conserv.*, vol. 29, no. 3, p. 158, 1984.

[93] F. Gherardi, “Efficient self-cleaning treatments for built heritage based on highly photo-active and well-dispersible TiO2 nanocrystals,” *Microchem J*, vol. 126, pp. 54–62, 2016.

[94] F. Gherardi, M. Roveri, S. Goidanich, and L. Toniolo, “Photocatalytic nanocomposites for the protection of European architectural heritage,” *Materials (Basel)*, vol. 11, no. 1, 2018.

[95] G. Cappelletti, P. Fermo, and M. Camiloni, “Smart hybrid coatings for natural stones conservation,” *Prog. Org. Coat.*, vol. 78, pp. 511–516, 2015.

[96] C. Kapridaki and P. Maravelaki-Kalaitzaki, “TiO2–SiO2–PDMS nano-composite hydrophobic coating with self-cleaning properties for marble protection,” *Prog. Org. Coat.*, vol. 76, no. 2–3, pp. 400–410, 2013.

[97] M. Abbate and L. D’Orazio, “Water diffusion through a titanium dioxide/poly(carbonate urethane) nanocomposite for protecting cultural heritage: Interactions and viscoelastic behaviour,” *Nanomaterials (Basel)*, vol. 7, no. 9, p. 271, 2017.

[98] M. F. La Russa *et al.*, “Nano-TiO2 coatings for cultural heritage protection: The role of the binder on hydrophobic and self-cleaning efficacy,” *Prog. Org. Coat.*, vol. 91, pp. 1–8, 2016.

[99] A. Chatzigrigoriou, I. Karapanagiotis, and I. Poulios, “Superhydrophobic coatings based on siloxane resin and calcium hydroxide nanoparticles for marble protection,” *Coatings*, vol. 10, no. 4, p. 334, 2020.

[100] J. Jeevanandam, A. Barhoum, Y. S. Chan, A. Dufresne, and M. K. Danquah, “Review on nanoparticles and nanostructured materials: history, sources, toxicity and regulations,” *Beilstein J. Nanotechnol.*, vol. 9, pp. 1050–1074, 2018.

[101] L. A. M. Carrascosa, R. Zarzuela, N. Badreldin, and M. J. Mosquera, “A simple, long-lasting treatment for concrete by combining hydrophobic performance with a photoinduced superhydrophilic surface for easy removal of oil pollutants,” *ACS Appl. Mater. Inter*, vol. 12, pp. 19974–19987, 2020.

[102] D. Aslanidou, I. Karapanagiotis, and C. Panayiotou, “Tuning the wetting properties of siloxane-nanoparticle coatings to induce superhydrophobicity and superoleophobicity for stone protection,” *Mater. Des.*, vol. 108, pp. 736–744, 2016.

[103] G. W. Scherer and G. S. Wheeler, “Silicate Consolidants for Stone,” *Key Eng. Mater.*, vol. 391, pp. 1–25, 2008.

[104] E. Franzoni, G. Graziani, E. Sassoni, G. Bacilieri, M. Griffa, and P. Lura, “Solvent-based ethyl silicate for stone consolidation: influence of the application technique on penetration depth, efficacy and pore occlusion,” *Mater Struct*.

[105] F. Sandrolini, E. Franzoni, and B. Pigino, “Ethyl silicate for surface treatment of concrete - Part I: Pozzolanic effect of ethyl silicate,” *Cem Concr Compos*, vol. 34, pp. 306–312, 2012.

[106] F. Xu and D. Li, “Effect of the addition of hydroxyl-terminated polydimethylsiloxane to TEOS-based stone protective materials,” *J Sol-Gel Sci Technol*, vol. 65, pp. 212–219, 2013.

[107] M. J. Mosquera, D. M. De Los Santos, and T. Rivas, “Surfactant-synthesized ormosils with application to stone restoration,” *Langmuir*, vol. 26, no. 9, pp. 6737–6745, 2010.

[108] C. Miliani, M. L. Velo-Simpson, and G. W. Scherer, “Particle-modified consolidants: A study on the effect of particles on sol–gel properties and consolidation effectiveness,” *J. Cult. Herit.*, vol. 8, no. 1, pp. 1–6, 2007.

[109] E. K. Kim, J. Won, J.-Y. Do, S. D. Kim, and Y. S. Kang, “Effects of silica nanoparticle and GPTMS addition on TEOS-based stone consolidants,” *J. Cult. Herit.*, vol. 10, no. 2, pp. 214–221, 2009.

[110] D. Li, F. Xu, Z. Liu, J. Zhu, Q. Zhang, and L. Shao, “The effect of adding PDMS-OH and silica nanoparticles on sol–gel properties and effectiveness in stone protection,” *Appl. Surf. Sci.*, vol. 266, pp. 368–374, 2013.

[111] Y. Luo, L. Xiao, and X. Zhang, “Characterization of TEOS/PDMS/HA nanocomposites for applica- tion as consolidant/hydrophobic products on sandstones,” *J Cult Herit*, vol. 16, no. 4, pp. 470–478, 2015.

[112] Y. Liu and J. Liu, “Synthesis of TEOS/PDMS-OH/CTAB composite coating material as a new stone consolidant formulation,” *Constr. Build. Mater.*, vol. 122, pp. 90–94, 2016.

[113] A. Torrisi, “Evaluation of five fluorinated compounds as calcarenite protectives,” *J. Cult. Herit.*, vol. 9, no. 2, pp. 135–145, 2008.

[114] L. R. Macheka-Tendenguwo, J. O. Olowoyo, L. L. Mugivhisa, and O. A. Abafe, “Per- and polyfluoroalkyl substances in human breast milk and current analytical methods,” *Environ. Sci. Pollut. Res. Int.*, vol. 25, no. 36, pp. 36064–36086, 2018.

[115] C. E. Lindemann, “Evaluation of Commercially Available Pfoa-Free Repellent Finishes,” NC State University, 2007.

[116] I. Ugur, “Surface characterization of some porous natural stones modified with a waterborne fluorinated polysiloxane agent under physical weathering conditions,” *J Coat Technol Res*, vol. 11, no. 4, pp. 639–649, 2014.

[117] D. Kronlund *et al.*, “Hydrophobization of marble pore surfaces using a total immersion treatment method – Product selection and optimization of concentration and treatment time,” *Prog. Org. Coat.*, vol. 85, pp. 159–167, 2015.

[118] Y. Cao, A. Salvini, and M. Camaiti, “Superhydrophobic fluorinated oligomers as protective agents for outdoor stone artworks,” *J. Cult. Herit.*, vol. 44, pp. 90–97, 2020.

[119] Z. Wang, I. T. Cousins, M. Scheringer, and K. Hungerbuehler, “Hazard assessment of fluorinated alternatives to long-chain perfluoroalkyl acids (PFAAs) and their precursors: Status quo, ongoing challenges and possible solutions, Environ,” *Environ. Int*, vol. 75, pp. 172–179, 2015.

[120] “Outdoor geology laboratory virtual tour – 2 marble,” *Wake Technical Community College*, 23-Mar-2022. [Online]. Available: https://www.waketech.edu/about-wake-tech/divisions/mathematics-sciences-engineering/departments/natural-sciences/geology/olg/2. [Accessed: 12-Nov-2022].

[121] “Get to know the most famous Greek quarries and their marbles,” *Stone Group International*. [Online]. Available: https://stonegroup.gr/blog/most-famous-greek-marble-quarries/. [Accessed: 12-Nov-2022].

[122] “Volatile organic compounds,” *Lung.org*. [Online]. Available: https://www.lung.org/clean-air/at-home/indoor-air-pollutants/volatile-organic-compounds. [Accessed: 12-Nov-2022].

[123] *Evonik.com*. [Online]. Available: https://corporate.evonik.com/en/products-and-solutions/industry-teams/bau/Products/protectos. [Accessed: 12-Nov-2022].

[124] *CIE, Publication CIE n&ordm 152, Colourimetry*. Vienna, 1986.

[125] R. Johnston-Feller, *Colour Science in the Examination of Museum Objects: Nondestructive Procedures, The Getty Conservation Institute*. Los Angeles, 2001.

[126] “PCE Instruments Colourimeter PCE-CSM 4,” *ProfiLab24 PCE Instruments Colourimeter PCE-CSM 4, 1.584,51€*. [Online]. Available: https://profilab24.com/en/laboratory/measurement-technology/pce-instruments-colourimeter-pce-csm-4?gclid=Cj0KCQiAgribBhDkARIsAASA5buuO8z865fbjaDjTGFZAZtYwb147tfy-IS5RwE690o0gkykWHNcDE4aAnb1EALw_wcB. [Accessed: 12-Nov-2022].

[127] L. Appolonia, V. Fassina, U. Matteoli, and A. M. Mecchi, “Methodology for the evaluation of protective products for stone materials. Part II: experimental tests on treated samples,” in *Methods of evaluating products for the conservation of porous building materials in monuments: preprints of the international colloquium*, Rome, 1995, pp. 301–316.

[128] P. Rizzarelli, C. La Rosa, and A. Torrisi, “Testing a fluorinated compound as a protective material for calcarenite,” *J. Cult. Herit*, vol. 2, pp. 55–62, 2001.

[129] A. Tsakalof, P. Manoudis, I. Karapanagiotis, I. Chryssoulakis, and C. Panayiotou, “Assessment of synthetic polymeric coatings for the protection and preservation of stone monuments,” *J. Cult. Herit*, vol. 8, pp. 69–72, 2007.

[130] Y. Lu, S. Sathasivam, J. Song, C. R. Crick, C. J. Carmalt, and I. P. Parkin, “Repellent materials. Robust self-cleaning surfaces that function when exposed to either air or oil,” *Science*, vol. 347, no. 6226, pp. 1132–1135, 2015.

[131] P. Wang, M. Chen, H. Han, X. Fan, Q. Liu, and J. Wang, “Transparent and abrasion-resistant superhydrophobic coating with robust self-cleaning function in either air or oil,” *J. Mater. Chem. A Mater. Energy Sustain.*, vol. 4, no. 20, pp. 7869–7874, 2016.

[132] Y. Guan *et al.*, “Design and fabrication of vapour-induced superhydrophobic surfaces obtained from polyethylene wax and silica nanoparticles in hierarchical structures,” *RSC Adv.*, vol. 8, no. 44, pp. 25150–25158, 2018.

[133] T. Yu *et al.*, “Ultra-durable superhydrophobic surfaces from 3D self-similar network via co-spraying of polymer microspheres and nanoparticles,” *Chem. Eng. J.*, vol. 410, no. 128314, p. 128314, 2021.

[134] *citation: NORMAL 43/93 - Misure colourimetriche di superfici opache*. .

[135] L. de Ferri, P. P. Lottici, A. Lorenzi, A. Montenero, and E. Salvioli-Mariani, “Study of silica nanoparticles – polysiloxane hydrophobic treatments for stone-based monument protection,” *J. Cult. Herit.*, vol. 12, no. 4, pp. 356–363, 2011.

[136] X. Zhu *et al.*, “Robust superhydrophobic surfaces with mechanical durability and easy repairability,” *J. Mater. Chem.*, vol. 21, no. 39, p. 15793, 2011.

[137] Q. Zhu *et al.*, “Robust superhydrophobic polyurethane sponge as a highly reusable oil-absorption material,” *J. Mater. Chem. A Mater. Energy Sustain.*, vol. 1, no. 17, p. 5386, 2013.

[138] I. Karapanagiotis, P. N. Manoudis, A. Savva, and C. Panayiotou, “Superhydrophobic polymer-particle composite films produced using various particle sizes,” *Surf. Interface Anal*, vol. 44, 2012.

[139] M. Reyes-Estebanez *et al.*, “Antimicrobial engineered nanoparticles in the built cultural heritage context and their ecotoxicological impact on animals and plants: a brief review,” *Herit. Sci.*, vol. 6, no. 1, 2018.

[140] F. Yu *et al.*, “Preparation and UV aging of nano-SiO2/fluorinated polyacrylate polyurethane hydrophobic composite coating,” *Prog. Org. Coat.*, vol. 141, no. 105556, p. 105556, 2020.

[141] M. Slavík, J. Bruthans, T. Weiss, and J. Schweigstillová, “Measurements and calculations of seasonal evapouration rate from bare sandstone surfaces: Implications for rock weathering,” *Earth Surf. Process.*, no. esp.4943, 2020.

[142] X. Gong and S. He, “Highly durable superhydrophobic polydimethylsiloxane/silica nanocomposite surfaces with good self-cleaning ability,” *ACS Omega*, vol. 5, no. 8, pp. 4100–4108, 2020.

[143] P. N. Manoudis, I. Karapanagiotis, A. Tsakalof, I. Zuburtikudis, B. Kolinkeová, and C. Panayiotou, “Superhydrophobic films for the protection of outdoor cultural heritage assets,” *Appl. Phys. A Mater. Sci. Process.*, vol. 97, no. 2, pp. 351–360, 2009.

[144] M. Ballester, R. Fort González, and M. Gomez-Heras, “Contributions of scanning electron microscopy to the assessment of the effectiveness of stone conservation treatments,” *Scanning*, vol. 26, pp. 41–47, 2004.

[145] P. Maravelaki-Kalaitzaki, N. Kallithrakas-Kontos, D. Korakaki, Z. Agioutantis, and S. Maurigiannakis, “Evaluation of silicon-based strengthening agents on porous limestones,” *Prog. Org. Coat.*, vol. 57, no. 2, pp. 140–148, 2006.

[146] M. Sadat-Shojai and A. Ershad-Langroudi, “Polymeric coatings for protection of historic monuments: Opportunities and challenges,” *J. Appl. Polym. Sci.*, vol. 112, no. 4, pp. 2535–2551, 2009.

[147] M. J. Mosquera, D. M. de los Santos, T. Rivas, P. Sanmartín, and B. Silva, “New nanomaterials for protecting and consolidating stone,” *J. nano res.*, vol. 8, pp. 1–12, 2009.

[148] E. Tesser, F. Antonelli, L. Sperni, R. Ganzerla, and N.-P. Maravelaki, “Study of the stability of siloxane stone strengthening agents,” *Polym. Degrad. Stab.*, vol. 110, pp. 232–240, 2014.

[149] M. Lettieri and M. Masieri, “Performances and coating morphology of a siloxane-based hydrophobic product applied in different concentrations on a highly porous stone,” *Coatings*, vol. 6, no. 4, p. 60, 2016.

[150] E. Ksinopoulou, A. Bakolas, and A. Moropoulou, *Modifying Si-based consolidants through the addition of colloidal nanoparticles. Appl. Phys. A.* 2016.

[151] I. Karapanagiotis, “Manoudis Superhydrophobic and Superamphiphobic Materials for the Conservation of Natural Stone: An Overview,” *Construction and Building Materials*, vol. 320, 2022.

[152] The European Committee for Standardisation (CEN), “Conservation of cultural property - Test methods - Determination of absorption by capillarity,” Slovenian Institute for Standardization, Jul. 2008.

[153] Z. Chughtai *et al.*, “A Superhydrophobic and Oleophobic Composite Coating for the Protection of Marble,” in *9th International Euro-Mediterranean Conference*, Limassol, Cyprus, 2022.

[154] H. Huang, H. Guo, and Y. Feng, “Study on UV-aging performance of fluorinated polymer coating and application on painted muds,” *Mater. Res. Express*, vol. 8, no. 1, p. 015301, 2021.

[155] European Committee for Standardization, “Conservation of Cultural Property - Test methods - Determination of water vapopur permeability,” 2009.